Water Resources Research

RESEARCH ARTICLE
10.1029/2021WR030119

Solving Challenges of Assimilating Microwave Remote Sensing Signatures With a Physical Model to Estimate Snow Water Equivalent

Ioanna Merkouriadi[1], Juha Lemmetyinen[1], Glen E. Liston[2], and Jouni Pulliainen[1]

[1]Finnish Meteorological Institute, Helsinki, Finland, [2]Colorado State University, Cooperative Institute for Research in the Atmosphere, Fort Collins, CO, USA

Key Points:

- Simulated snow properties from SnowModel are used in microwave-based snow water equivalent (SWE) retrievals by MEMLS3&a
- Biases in physically modeled SWE can induce larger biases in microwave-based SWE retrievals
- The challenges can be mitigated when microwave algorithms account for the physical relationship of snow properties

Correspondence to:
I. Merkouriadi,
Ioanna.merkouriadi@fmi.fi

Citation:
Merkouriadi, I., Lemmetyinen, J., Liston, G. E., & Pulliainen, J. (2021). Solving challenges of assimilating microwave remote sensing signatures with a physical model to estimate snow water equivalent. *Water Resources Research*, *57*, e2021WR030119. https://doi.org/10.1029/2021WR030119

Received 1 APR 2021
Accepted 18 OCT 2021

Author Contributions:
Conceptualization: Ioanna Merkouriadi, Juha Lemmetyinen
Formal analysis: Ioanna Merkouriadi, Juha Lemmetyinen
Funding acquisition: Juha Lemmetyinen
Investigation: Ioanna Merkouriadi, Juha Lemmetyinen
Methodology: Ioanna Merkouriadi, Juha Lemmetyinen
Project Administration: Juha Lemmetyinen
Resources: Juha Lemmetyinen
Software: Ioanna Merkouriadi, Juha Lemmetyinen
Supervision: Juha Lemmetyinen, Glen E. Liston, Jouni Pulliainen
Validation: Ioanna Merkouriadi, Juha Lemmetyinen

Abstract Global monitoring of seasonal snow water equivalent (SWE) has advanced significantly over the past decades. However, challenges remain when estimating SWE from passive and active microwave signatures, because a priori characterization of snow properties is required for SWE retrievals. Numerical experiments have shown that utilizing physical snow models to acquire snowpack characterization can potentially improve microwave-based SWE retrievals. This study aims to identify the challenges of assimilating active and passive microwave signatures with physical snow models, and to examine solutions to those challenges. Guided by observations from a point-based study, we designed a sensitivity experiment to quantify the effects of changes in the physically modeled SWE—and of corresponding changes to other snowpack properties—to the microwave-based SWE retrievals. The results indicate that assimilating microwave signatures with physical snow models face some critical challenges associated with the physical relationship between SWE and snow microstructure. We demonstrate these challenges can be overcome if the microwave algorithms account for these relationships.

1. Introduction

Seasonal snow critically affects the terrestrial energy balance of snow-covered areas, due to its high optical reflectivity and low thermal conductivity. Therefore, it affects numerous climate-related interactions among the atmosphere, hydrosphere, and biosphere (Liston & Hiemstra, 2011; Mudryk et al., 2017; Shi et al., 2011; Wrzesien et al., 2018). In addition to its crucial role in the climate system, snow is an important freshwater reservoir. An estimated one-sixth of Earth's population lives in areas where the primary source of freshwater is snow (Barnett et al., 2005). Knowledge of seasonal snow mass is vital for numerous applications spanning from freshwater management to climate projections, such as estimating seasonal energy production via hydropower, improving medium and long-range weather forecasts, and validating Global Circulation Models (Aas et al., 2017; Foster et al., 1994; Li et al., 2018; Zhu et al., 2019).

Estimating the mass of seasonal snow cover, i.e., the snow water equivalent (SWE), on a global scale remains a challenge. To this day, the most widely used Earth observation products are passive microwave sensors that offer daily global coverage of SWE for the past 40 years (Gonzalez & Kummerow, 2020; Pulliainen et al., 2020; Tedesco & Narvekar, 2010). Long-term global coverage is appealing, but it comes with two critical challenges. First, the resolution of passive microwaves is coarse (e.g., 25 km pixels), increasing retrieval uncertainty over heterogeneous landscapes. Second, microwave signals are not only affected by the snow mass, that is, snow depth and density, but also by a handful of snow properties and structural parameters, such as snow layering, microstructure, temperature, and moisture, hereafter referred to as *snowpack states*. Numerous microwave radiative transfer models have been developed to describe the relationship between snowpack states and microwave signatures (e.g., Picard et al., 2018; Proksch et al., 2015; Pulliainen et al., 1999; Tan et al., 2015; Wiesmann & Mätzler, 1999; Zhu et al., 2018) collected by both active and passive sensors (radars and radiometers). However, continuous and reliable representation of the snowpack states required to drive these models is a major challenge. Active microwave sensors, for example Synthetic Aperture Radars, are a promising alternative because they can overcome the coarse resolution of passive microwave sensors, and thus mitigate the first challenge. Even so, the second challenge remains: a priori characterization of the snowpack states is imperative for reliable SWE retrievals from passive or active microwave signals (Dai, et al., 2012; Davenport et al., 2012; Durand & Liu, 2012; Lemmetyinen et al., 2018).

Writing – original draft: Ioanna Merkouriadi
Writing – review & editing: Juha Lemmetyinen, Glen E. Liston, Jouni Pulliainen

An alternative method for estimating SWE is through physical models. High-resolution snow evolution models can capture key snow processes, heterogeneities, and interactions between snow and land cover, allowing for improved snow representation and better understanding of the snowpack states. Advancements in computational power, together with the increased quality and availability of topographic, land cover, and meteorological data products, make physical snow models ideal candidates for global scale snow monitoring (Brown & Mote, 2009; Brun et al., 2013; Liston & Hiemstra, 2011). However, they also come with a major challenge: they rely on continuous and reliable weather forcing data sets. Despite improvements of atmospheric reanalysis products, reliable winter precipitation amounts remain a challenge (Boisvert et al., 2018; Lindsay et al., 2014), potentially leading to large uncertainties in global scale SWE retrievals. In fact, reanalysis data-based SWE products exhibit a systematic change of bias as a function of time deteriorating their feasibility to inform climate trend analysis (Pulliainen et al., 2020). From an operational (real-time) point of view, precipitation forcing comes from numerical weather products or real-time precipitation analyses that also come with large uncertainties (Maggioni et al., 2016).

Several case studies have emphasized the strong potential of combining methods between the two most valuable tools for SWE monitoring: microwave remote sensing and snow physical modeling; This can be done either by assimilating remote sensing products of SWE with land surface models directly (De Lannoy et al., 2010), or by assimilating microwave signatures (backscatter, brightness temperature) with physical models through a forward model which acts as an observation operator (e.g., Durand et al., 2009; Kontu et al., 2017; Langlois et al., 2012; Larue et al., 2016). The aim of this study is to identify the challenges of assimilating microwave signatures with physical snow models, and to provide solutions. We used a state-of-the-art snow evolution model (SnowModel, Liston & Elder, 2006a; Liston et al., 2020) to drive a semiempirical radiative transfer model (microwave emission model for layered snowpacks; MEMLS3&a, Proksch et al., 2015; henceforth MEMLS), to produce a set of synthetic observations of passive (brightness temperature) and active (backscatter) microwave signatures. The synthetic microwave observations were evaluated against tower-based observations from a measurement site in Northern Finland. We then conducted a sensitivity experiment to quantify the effects of changes in the physically modeled SWE—and of corresponding changes in all snowpack states—to the microwave-based SWE retrievals. Synthetic observations were used in place of real observations to remove random biases between model estimates and microwave observations. Once the challenges were identified, we examined solutions for practical retrieval applications. In addition, we discuss the applicability of our point-based approach in large scale applications.

2. Materials and Methods

In this section, we briefly introduce the physical snow evolution model (SnowModel, Section 2.1) and the radiative transfer model (MEMLS, Section 2.2) used in this assimilation study. The simulation setup of both models is described in Section 2.3. In Section 2.4, we describe the microwave and in situ observations that guided this study. The experimental design used to identify the assimilation challenges is described in Section 2.5. Finally, in Section 2.6, we present the methodology of potential solutions to the challenges derived in the previous section. Methodology in Section 2.6 can be better interpreted after identifying limitations in the coupled model in Section 3.3.

2.1. The Physical Snow Evolution Model (SnowModel)

SnowModel (Liston & Elder, 2006a; Liston et al., 2020) is a modeling system comprised of five numerical sub-models that simulate all first-order processes that govern the seasonal evolution of snow depth, snow density, blowing-snow redistribution and sublimation, snow grain size, and thermal conductivity, in a spatially distributed, time-evolving, multi-layer snowpack framework. The SnowModel components include: (a) quasi-physically based, high-resolution, meteorological forcing distributions (MicroMet; Liston & Elder, 2006b); (b) simulations of the surface energy balance (EnBal; Liston & Hall, 1995; Liston et al., 2007); (c) calculation of multi-layer snow properties including snow depth, density, temperature, and SWE (SnowPack-ML; Liston & Hall, 1995; Liston & Mernild, 2012); (d) representation of blowing-snow processes (SnowTran-3D; Liston & Sturm, 1998; Liston et al., 2007); and (e) assimilation of ground-based and remotely sensed snow property observations (SnowAssim; Liston & Hiemstra, 2008). SnowModel is designed to run on spatial increments of 1 m to 10s of km, with a temporal resolution of 10 min to 1 day.

SnowModel can reproduce high-resolution spatial distributions of snow properties, given topography and vegetation information over a spatial domain of interest. This feature is not fully exploited here because our study is based on a spatially confined experiment, and the snowpack around the study area is quite uniform. Nevertheless, this is a valuable feature regarding synergies between SnowModel and microwave models on satellite scales.

A brief overview of the SnowModel main components follows, with emphasis on the physics related to this assimilation study.

2.1.1. MicroMet

MicroMet is a downscaling model designed to provide high-resolution meteorological forcing distributions in response to prescribed meteorological data, from either adjacent meteorological stations or assimilated atmospheric reanalysis data. These distributions are required when simulating spatial distributions of snow properties. MicroMet outputs include air temperature, relative humidity, wind speed and direction, incoming solar radiation, incoming longwave radiation, surface pressure, and precipitation. If solar and longwave radiation are not prescribed, they are calculated by MicroMet.

2.1.2. EnBal

EnBal calculates the energy balance between the snow surface and the atmosphere. Surface temperature together with energy and moisture fluxes are simulated in response to the atmospheric conditions provided by MicroMet. The surface energy balance model (Equation 1) is dependent on the incoming solar radiation Q_{si}, the surface albedo α_s, the incoming Q_{li} and emitted Q_{le} longwave radiation at the surface, the turbulent exchanges of latent Q_e and sensible Q_h heat, the conductive heat flux Q_c, and the residual energy available for melt Q_m:

$$\left(1-\alpha_s\right)Q_{si}+Q_{li}+Q_{le}+Q_h+Q_e+Q_c=Q_m \tag{1}$$

Surface temperature T_0 is the only unknown variable, thus the surface energy balance equation is solved iteratively for T_0. In snow presence if $T_0 > 0°\mathrm{C}$, it indicates there is energy available for melting. T_0 is then fixed to 0 and the energy balance is solved for Q_m.

Surface albedo of non-melting snow can be time-dependent, depending on how SnowModel is configured, and is different below forest canopies, forest-free areas, and for glacier ice.

2.1.3. SnowPack-ML

SnowPack-ML is based on the SnowPack sub-model under SnowModel framework (Liston & Hall, 1995), reconfigured in a multilayer framework. SnowPack is an evolution model that describes the changes in snow depth and SWE in response to the precipitation and melt fluxes defined by MicroMet and EnBal. Snow density evolves in response to the weight of the overlying snow (compaction), snow temperature, sublimation of non-blowing snow, and melting. Snow melt decreases the snow depth, and the associated meltwater is redistributed in the snowpack until the snow density reaches a maximum threshold value. Wind slabs are simulated in response to wind speed variations (Liston et al., 2007, 2020).

The density increase due to compaction follows Anderson (1976):

$$\frac{\partial \rho_s}{\partial t}=A_1 h_w^* \rho_s \exp\left[-B\left(T_f-T_s\right)\right]\exp\left(-A_2\rho_s\right) \tag{2}$$

where ρ_s (kg m^{-3}) is the snow density, $h_w^*=\left(1/2\right)h_w$ (m) is the snow weight defined as half of the SWE h_w (m), T_f (K) is the freezing temperature of water, and T_s (K) is the snow temperature. $A_1 = 0.0013$ m^{-1}, $A_2 = 0.021$ m^3 kg$^{-1,}$ and $B = 0.08$ K^{-1} are constants based on Kojima (1967). The SWE is defined to be:

$$h_w=\frac{\rho_s}{\rho_w}\zeta_s \tag{3}$$

where ρ_w (kg m^{-3}) is the water density, and ζ_s (m) is the snow depth.

In SnowPack-ML, each snowfall event creates a new snow layer, mimicking the snow stratigraphy found in nature. The user defines the maximum number of snow layers, albeit there is no numerical limitation. There is an algorithm in SnowPack-ML that merges thin and thermodynamically unimportant snow lay-

ers, in order to prevent the number of layers from exceeding the predefined maximum. A recent feature of SnowPack-ML is the parameterization of grain size (Liston et al., 2020). Grain growth is parameterized by a snow-structure sub-model that is part of SNTHERM model (Jordan, 1991). Snow grains grow in response to snowpack temperature gradients, and thus vapor pressure gradients, and snow density. The evolution of snow grain diameter (D) is given by:

$$\frac{\partial D}{\partial t} = \frac{g_1 \left| U_v \right|}{D} \tag{4}$$

where t (s) is time, U_v (kg m^{-2} s^{-1}) is the mass vapor flux and the parameter $g_1 = 5.0 \times 10^{-7}$ m^4 kg^{-1}. The mass vapor flux is defined to be:

$$U_v = -\psi D_{es} C_{iT} \frac{\partial T}{\partial z} \tag{5}$$

where D_{es} (m^2 s^{-1}) is the effective diffusion coefficient for snow, C_{iT} (kg m^{-3} K^{-1}) is the ice equilibrium vapor variation with temperature, T (K) is the snow temperature, and z (m) is the snow depth. D_{es} is given by:

$$D_{es} = D_{e0s} \left(\frac{1.0 \times 10^5}{P} \right) \left(\frac{T}{T_m} \right)^6 \tag{6}$$

where P (Pa) is the atmospheric pressure, T_m (= 273.15 K) is the melting temperature, and D_{e0s} (9.2×10^5 m^2 s^{-1}) is the effective diffusion coefficient at $P = 1.0 \times 10^5$ Pa and $T = 0°C$. C_{iT} is given by:

$$C_{iT} = \frac{c_{1i}}{T^2} \left(\frac{L_{vi}}{R_w T} - 1 \right) e^{-\left(L_{vi} / R_w T \right)} \tag{7}$$

where $c_{1i} = 7.964 \times 10^9$ kg K m^{-3}, L_{vi} (=2.838 × 10^6 J kg^{-1}) is the latent heat of sublimation of ice, and R_w (=461.5 J K^{-1} kg^{-1}) is the gas constant for water vapor.

In contrast to Jordan (1991), SnowPack-ML assumes that vapor fluxes are proportional to the porosity of the snowpack. This means that the vapor flow is reduced in denser snow.

2.1.4. SnowTran-3D

SnowTran-3D is a three-dimensional sub-model that calculates wind-driven snow-depth evolution. The primary components of SnowTran-3D are: (a) the wind forcing field, (b) the wind shear stress on the surface, (c) the snow transport by saltation and suspension, (d) the sublimation of saltated and suspended snow, and (e) the accumulation and erosion of snow at the surface. Vegetation information is essential when simulating wind-blown snow, so each grid cell has information on vegetation type. There are 24 predefined vegetation types that are assigned a canopy height. The canopy height equals the so-called snow-holding depth. Snow becomes available for wind transport when snow depth exceeds the snow-holding depth.

2.1.5. SnowAssim

SnowAssim model is a data assimilation scheme used to calculate the difference between modeled and observed SWE distributions (Liston & Hiemstra, 2008). One, or more, observations of SWE are provided at specific time steps. SnowAssim calculates the difference between the observed and simulated SWE values at these time steps. Based on the differences, the model calculates adjustment factors that are used to modify precipitation and melting over the whole period preceding the SWE observation, in order to reproduce the observed SWE.

2.2. The Radiative Transfer Model (MEMLS)

MEMLS approximates the snowpack as a stack of planar horizontal layers. Model input parameters for each layer include layer thickness, temperature, density, liquid water content, salinity, and correlation length. In this study, salinity of snow is always considered to be zero. The snow scattering coefficient is determined by the frequency used, and the density and correlation length of the snow layer. Equations are derived either from empirical observations of snow sample measurements (Wiesmann et al., 1998) or based on the Improved Born Approximation for coarse grain size (IBA, Mätzler & Wiesmann, 1999). Internal volume scattering is consid-

ered through a two-flux approximation of a six-flux model (Wiesmann & Mätzler, 1999). The radiative transfer in MEMLS accounts for internal refraction and reflection processes in the snowpack. As a simplification, the propagation directions of radiation are reduced to six fluxes streaming along and opposed to the three principal axes. Trapped radiation is presented by the horizontal fluxes. Up- and downwelling radiation are a function of the six-flux parameters. MEMLS takes into account several effects related to evenly layered structures of media; a combination of coherent and incoherent treatment is used to calculate reflection, transmission, and refraction coefficients between layer interfaces. Essentially, coherent treatment is applied when the layer thickness approaches a quarter of the simulated wavelength. MEMLS also calculates an effective propagation angle in the snowpack to complement the refraction angle given directly by Fresnel equations. The effective angle is calculated as a combination of the refraction angle as given by Snell's law and the primary direction of volume scattering within the snowpack. The effect becomes significant as volume scattering increases, affecting the higher frequencies more. Also, the reflectivity values at layer interfaces are modified by the theoretical effects of polarization mixing. Upwelling brightness temperature from the stacked system of snow layers and ground is solved by simulating the extinction of upwelling radiation from the ground, self-emission and extinction of radiation from the snow medium, as well as the extinction and reflection of downwelling radiation from the sky.

Based on the same physical principles as the original model, an extension to MEMLS to calculate microwave backscatter was published by Proksch et al. (2015). In the derived "MEMLS3&a" model for backscatter, surface reflectivity is decomposed into diffuse and specular components, also taking into account slight undulations of the snow surface. These parameters have to be defined separately. The calculation of cross-polarization is similarly based on an empirical relation to like-polarized backscatter, which is defined by the user. Backscattering from the stacked snow-ground system is solved by calculating the propagation of emitted radiation in the reverse direction, taking into account scattering and extinction in snow layers as well as reflections at medium interfaces.

2.3. Simulation Setup for SnowModel and MEMLS

SnowModel simulations were performed using meteorological forcing data from an automatic weather station in northern Finland, located in the proximity of our study area (67.366618°N, 26.628976°E). Air temperature, relative humidity, precipitation, and wind speed and direction have been measured at the weather station since 2006 (https://litdb.fmi.fi/luo0015_data.php). The wind speed sensor is located above the canopy, at 22 m height. Wind speed modifications provided by Essery et al. (2016) were used to meet SnowModel requirements. SnowModel simulations were performed with assimilation of SWE, to correct for possible SWE biases due to, e.g., underestimation of precipitation in the meteorological forcing data, and to better reflect the observed conditions. In situ SWE observations from mid-March were used for assimilation. Annual SWE observations were 164, 140 and 176 mm for the years 2010, 2011, and 2013, respectively. SnowModel simulations were conducted using a 3 hr time step and a 12-layer maximum snowpack setup, allowing the simulation to reflect the naturally evolved multiple-layers observed at the site, while limiting the computational stress imposed on microwave emission and backscatter simulations. Hereafter, we refer to this SnowModel run as the *base run*. The base run started on July 1, 2009 and run through June 30, 2013.

SnowModel currently predicts the mean grain diameter (D) as the snow microstructural parameter based on SNTHERM, while MEMLS requires an estimate of the snow exponential (auto) correlation length (l_{exp}). Thus, prior to inserting SnowModel estimates of grain size in MEMLS, the empirical conversion proposed by Wiesmann et al. (2000) was applied:

$$l_{\mathrm{exp}} = 0.16 * D \tag{8}$$

The study by Wiesmann et al. (2000) focused in utilizing physically modeled snow properties, such as snow microstructure, in MEMLS to simulate microwave radiation. Two physical models, Crocus (Météo France, 1996) and SNTHERM were used for that purpose. The linear relationship (Equation 8) was obtained after comparing SNTHERM computed profiles of grain diameter to in situ snowpit profiles.

The contribution of the ground surface to the observed backscattering and emission was estimated by empirically fitting early season MEMLS simulations to observations, where the influence of snow on the microwave signal was minimal. Because early season observations were not available for all seasons, parameters acquired for the second season were applied across all years; the period between November 8 and 13,

Table 1
MEMLS Simulation Parameters for Different Frequencies

Frequency	13.4 GHz	16.7 GHz	18.7 GHz	36.5 GHz
Polarization	VV	VV	V	V
Simulated quantity	Backscatter		Brightness temperature	
Ground temperature (K)	NA	NA	272	272
Downwelling sky brightness temperature (K)[a]	NA	NA	15	35
Ground reflectivity [b](vertical polarization)	0.05	0.047	0.045	0.045
Fraction of specular scatter[b]	0.69	0.35	NA	NA
Incidence angle	50			
Scattering model	IBA			

[a]Downwelling sky brightness temperature calculated using statistical model (Pulliainen et al., 1993). [b]Ground reflectivity values were based on optimizing model simulations for early season.

2010 was chosen. During this period, a snowpack of ~10 cm was already present, so parameters given by SnowModel were used in MEMLS during iteration of the ground parameters. Another option would have been to apply observations from completely snow-free conditions available e.g., from the second year, but this period showed high variability in both measured backscatter and brightness temperature (TB). This was attributed to changes in ground permittivity induced by variations in soil moisture. For the TB simulations, the ground reflectivity was iterated to achieve a match between simulated and observed values, assuming a ground temperature of 272 K. For the backscatter simulations, realistic soil reflectivity values were combined with an iteration of the portion of specular and diffuse scatter to achieve the match. The downwelling sky brightness temperatures are calculated using a statistical model (Pulliainen et al., 1993) using typical atmospheric parameters for winter conditions in Finland. Ancillary parameters and model settings used in MEMLS are summarized in Table 1.

MEMLS simulations of backscatter and brightness temperature were performed for each time step when simulated snowpack states were available from the base run, creating a synthetic set of microwave observations. The synthetic observations were compared to the real observations of backscatter and brightness temperatures. The results are summarized in Section 3.1.

2.4. Microwave and in Situ Observations From the Study Area

Microwave and in situ observations from the NoSREx campaign (2009–2013; Lemmetyinen et al., 2016) were used to evaluate MEMLS and SnowModel predictions. The NoSREx campaign was designed to provide passive and active microwave observations of snow conditions representative of the boreal forest zone (Lemmetyinen et al., 2018, 2016). It was coordinated by the Arctic Research Center of the Finnish Meteorological Institute, and it took place in Sodankylä, northern Finland (67.368°N, 26.633°E). Sodankylä is seasonally covered by snow that lasts, on average, 200 days per year, from October to May (Merkouriadi et al., 2017; Pirinen et al., 2012). The annual maximum snow depth occurs in March and averages over 80 cm (Essery et al., 2016; Merkouriadi et al., 2017). In winter, soil freezing depth exceeds 2 m (Rautiainen et al., 2014) and air temperatures can drop below −30°C. The snow conditions in Sodankylä are typical of a boreal forest snowpack (Leppänen et al., 2015; Sturm et al., 1995). The NoSREx measurement site (Intensive Observation Area [IOA]) was located in a clearing amidst a pine forest, 7 km southeast from the town of Sodankylä. The ground at the site consists of sandy mineral soil covered by a thin organic layer, and low vegetation including shrubs, grass, and lichen.

2.4.1. Microwave Observations

Two tower-based microwave instruments collected continuous microwave observations over four years, 2009–2013. In this study, data from years 2010, 2011, and 2013 are used; microwave measurements in 2012 started late in the season due to problems with instruments (Lemmetyinen et al., 2016) and are left out of the analysis here. The active instrument, SnowScat, is a fully polarimetric radar that operates on frequencies

from X-to Ku bands (Werner et al., 2010). The passive instrument, SodRad, is a commercial, dual-polarization radiometer system with four modular, dual-polarization receivers operating from X-to W bands. The instruments were deployed on separate towers, but overlooking the same forest clearing.

SnowScat was installed at an elevation of 9.6 m above ground level. A positioner device allowed scans of the test area in both azimuth and elevation; scans were performed at four elevation angles (at 60°, 50°, 40°, and 30° from Nadir), acquiring independent looks from 17 discrete azimuth directions. Each data acquisition consisted of measurements at four polarizations (VV, VH, HV, and HH) over the whole frequency range of the instrument, as well as a measurement of an internal calibration path. Scans were made nominally every three hours during the first seasons and every four hours in consecutive seasons. In post-processing, the single-look complex data were sampled to three 2 GHz bands with center frequencies at 10.2, 13.4, and 16.7 GHz. An average over the azimuth scan was further taken to reduce radar speckle, yielding a single backscattering value corresponding to each elevation for a given scan. Calibration stability was verified by measuring an external calibration target (sphere) before and after each azimuth-elevation scan sequence. The instrument stability for all four seasons of NoSREx was estimated to be ±1 dB (Lemmetyinen et al., 2016).

SodRad was installed on a separate platform at a height of 4.1 m overlooking the IOA. From 2009 through 2012, receivers at 10.65, 18.7, 37, and 90 GHz were applied. In 2012, the 90 GHz receiver was replaced by a 21 GHz receiver. The nominal SodRad measurement sequence consisted of scans in elevation at 5° steps from 30° to 70° off the nadir. A noise injection technique is used to calibrate SodRad measurements internally, while absolute calibration was performed using two external loads. Calibration stability was verified by performing measurements of the sky between scans; calibration stability was estimated to be better than 2 K for all channels over the snow season.

In this study, we apply data from SodScat at VV polarization at 13.4 and 16.7 GHz for evaluating model predictions. The 10.2 GHz band was omitted because it showed minimal response to dry snow (Lemmetyinen et al., 2018). The cross-polarized data was omitted from evaluations since the forward model applied in the study (MEMLS) calculates cross-polarized backscatter directly from the co-polarized signal using a scaling factor. SodRad data at 18.7 and 37 GHz, vertical polarization, were applied in similar evaluations of passive microwave simulations. These are typically the frequencies used for passive microwave SWE remote sensing, with the vertical polarization being less sensitive to ice layers and crusts within the snowpack, when compared to the horizontal polarization (Rees et al., 2010).

2.4.2. In Situ Observations of Snow Properties

Snow-pit measurements were taken once a week from the IOA (twice a week for the first season), in the proximity of the microwave measurement platforms. New pits were made at a minimum distance of 1 m from previous pits, to ensure an undisturbed snowpack. Detailed snow properties measured in the field included snow depth and SWE, together with profiles of temperature, density, moisture, stratigraphy (layering), snow grain size, and grain type. Temperature, density, and moisture were measured at 10 cm intervals. A precision digital thermometer was used to record temperature. Density was measured both using a manual density cutter, and the SnowFork instrument (Sihvola & Tiuri, 1986). Data for 2009 density profiles consist mostly of SnowFork measurements. Moisture was measured using the SnowFork. For the snow microstructure, grain size, and type assessment, a sample was taken from each visually identified snow layer. Grain size and type were analyzed in post-processing from macro photographs of the snow samples taken against a reference grid. The traditional snow grain size, defined as the largest diameter of a typical particle (Colbeck, 1990; Fierz et al., 2009), was recorded for each layer. The measurement methods are described in detail by Leppänen et al. (2016).

2.5. Identifying Assimilation Challenges—A Sensitivity Experiment

In physical snow modeling, changes in SWE affect several snow properties, including all snowpack states required in microwave-based SWE retrieval algorithms: snow microstructure, depth, temperature, and density. Microwave models are especially sensitive to snow microstructure. When considering synergies between physical snow models and microwave models, it is crucial to examine and quantify how biases in physically

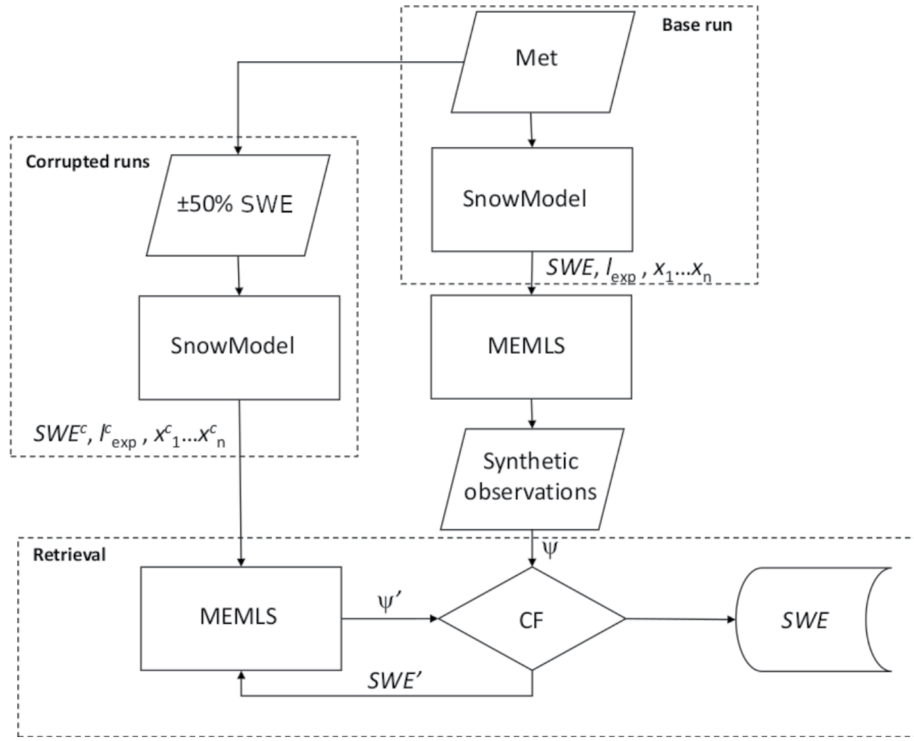

Figure 1. Flowchart of the sensitivity experiment scheme.

modeled SWE, and corresponding changes in all related snowpack states, will affect microwave-based SWE retrievals. We developed the following sensitivity experiment (Figure 1) to address that question.

In addition to the base run which was used as a basis of our synthetic set of observations (Ψ), we performed 10 more SnowModel simulations, in which we perturbed end-of-season SWE in a controlled manner (±10%–50%, in 10% increments). The SWE perturbations were produced by applying the SnowAssim model described in Section 2.1. Specifically, in each year we perturbed an in situ SWE observation in late March from ±10% to ±50%, in 10% increments. For each perturbation, SnowAssim calculated adjustment factors that were applied iteratively to precipitation/melting over the whole snow accumulation season prior to the SWE observation to achieve the perturbed SWE in late March.

Each of the perturbed simulations predicted snowpack states at a 3 hr time step. The derived "perturbed" SWE (SWE^c), correlation length (l^c_{exp}), and properties x^c_n of each layer i were used to simulate observables (Ψ') using MEMLS. A local minimum of a cost function was searched numerically using the Nelder-Mead method, comparing MEMLS simulated values against the synthetic observations (Ψ), using snow depth as a minimization parameter. We used the synthetic microwave observations to remove the effect of uncertainties related to the real observations, and to gain control over the sensitivity experiment.

Because a multiple-layer snowpack representation is used, the inversion algorithm produces scaling factors that are applied to the depth of each layer, so that together with a fixed density, each layer yields a SWE value. A common scaling factor is applied across the whole snowpack. A similar scaling factor can be applied to the correlation length of each layer. Assuming that both observation errors and the uncertainty of the correlation length estimate are normally distributed, the general cost function takes the form:

$$\mathrm{CF}\left(\alpha,\beta\right)=\sum_{i=1}^{I}\frac{\left[\Psi_i'\left(\alpha\cdot\mathrm{SWE}_{\mathrm{SM}},\beta\cdot l_{\mathrm{exp,SM}},x_1,\ldots x_n\right)-\Psi_i\right]^2}{2\sigma_i}+\frac{\left[\alpha-\alpha_{\mathrm{ref}}\right]^2}{2\sigma_{\alpha,\mathrm{ref}}}+\frac{\left[\beta-\beta_{\mathrm{ref}}\right]^2}{2\sigma_{\beta,\mathrm{ref}}} \quad (9)$$

where $x_1,\ldots x_n$ are ancillary model parameters, α and β are the scaling factors of layer height and correlation length, α_{ref} and β_{ref} the reference values of the scaling factors, $\sigma_i$is the variance of observation Ψ_i, and $\sigma_{\alpha,ref}$ and $\sigma_{\beta,ref}$ the variance of the scaling factors α and β. The reference value of the scaling factors is set as

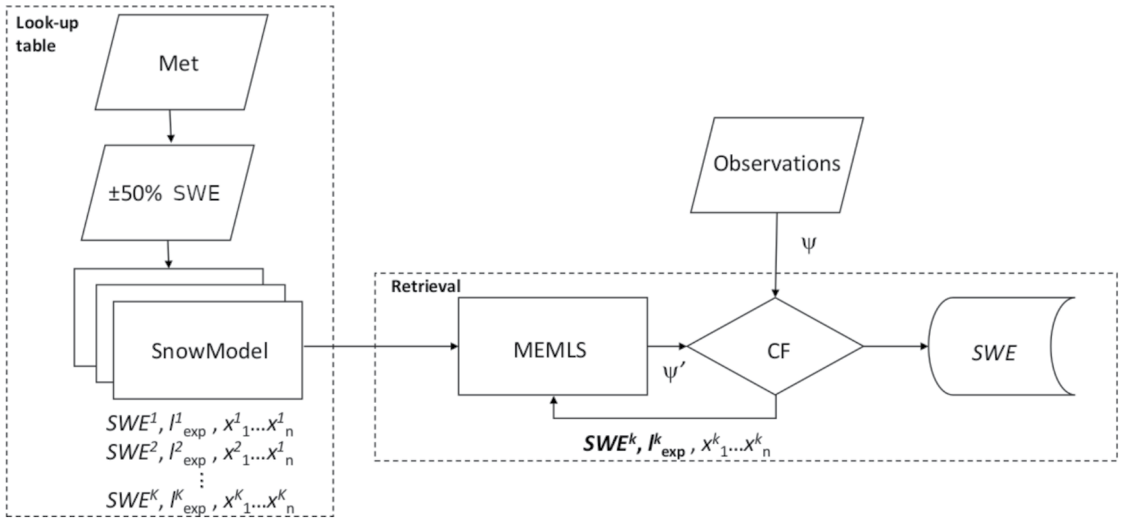

Figure 2. Flowchart of the look-up table scheme.

$\alpha_{ref} = \beta_{ref} = 1$ to match the reference value to the original SnowModel output. Therefore, the variance of the scaling factors denotes the magnitude of deviation allowed from the initial values given by SnowModel (SM).

In active microwave retrievals, observations of two channels (13.4 and 16.7 GHz, VV-pol) were applied in the cost function as individual observations ($i = 2$). The motivation for this was to demonstrate a combination of frequencies close to recently proposed satellite missions (e.g., Derksen et al., 2019). For passive microwaves, the channels 18.7 and 36.5 GHz were similarly applied ($i = 2$) as individual channels, in place of the more typical channel difference (18.7–36.5 GHz). Applying a channel difference negates some of the effect of snow and ground temperature variations, which is beneficial in a typical retrieval environment where information on physical temperature is not available (e.g., Kelly et al., 2003). Here, since also the temperature of each snow layer was available from SnowModel, the channels were applied individually.

The uncertainty (variance) of backscattering observations is assumed to be 1 dB, while the uncertainty of brightness temperatures is assumed at 2 K. Because constant variances are used for all remote sensing observations, the choice of scaling factor uncertainty largely determines how closely the retrieval follows the initial values predicted by SnowModel. The variances of the scaling factors were applied here only to either fix a given parameter to the reference value ($\sigma_\alpha, \sigma_\beta \ll 1$) or setting the parameter free in the iteration ($\sigma_\alpha, \sigma_\beta \gg 1$).

In the sensitivity experiment, retrievals were performed by setting snow depth as a free parameter ($\sigma_\alpha \gg 1$), and fixing all other parameters, including the microstructure (l_{exp}), to the SWE-perturbed SnowModel runs ($\sigma_\beta \ll 1$). This emulates an approach used in microwave-based SWE retrievals, where a given microstructure value is kept constant while the cost function is minimized by fluctuating snow depth (as done by e.g., Takala et al., 2011). In that manner, we were able to identify the challenges of inducing modeled snowpack states to the microwave-based SWE retrievals, when the physical relationship between these parameters is not maintained.

2.6. Proposing Solutions to the Assimilation Challenges

2.6.1. Look-Up Tables

To account for the physical relationship between the snowpack states, we designed a scheme based on a simplified, look-up table approach (Figure 2). We should note that previous work utilizing look-up tables have typically applied arbitrary combinations of snow characteristics, for example, a range of snow depths, densities and microstructure, to generate look-up tables of remote sensing observables (backscatter, brightness temperature), enabling rapid inversion of a forward model (e.g., Zhu et al., 2018). Furthermore, for

example, Dai et al. (2012) applied empirically generated relations for snow characteristics (density, grain size, and number of layers) to generate look-up tables of brightness temperature where initial snow characteristics are determined based on date. However, in this study, we generate look-up tables of SnowModel solutions of snowpack states for a range of perturbation in the SWE. The look-up tables thus describe physically modeled snow characteristics at a given moment of time for a given SWE, differing from previous works where this physical connection was missing; for example, in the study by Dai et al. (2012), snow density and grain size were determined only by the date.

We conducted 20 SWE-perturbed SnowModel runs within the range of ±50% of the base run SWE, in ±5% intervals. Based on these runs, we created look-up tables consisting of simulated groups of SWE and other snowpack states. For retrieving SWE at a given time step, the snowpack states were used to drive MEMLS, and the cost function was applied to determine the group providing a minimum difference to observations. In order to demonstrate the method, we used synthetic microwave observations in place of real observations, only this time we added normally distributed random noise corresponding to the combined uncertainty of measurements and MEMLS forward simulations (standard deviations of 2, 4, 6, 8, and 10 K for brightness temperature and 0.2, 0.4, 0.6, 0.8, and 1 dB for backscatter). A Monte Carlo approach was adopted, generating 100,000 variations of the synthetic observations at each noise level; noise was applied independently for each channel. In this experiment, both co- and cross-polarized synthetic observations (VV and VH) were applied in active microwave retrievals. Retrievals with co-polarized observations alone resulted in high sensitivity to observation uncertainty (not shown). The addition of cross-polarized synthetic observations inherently reduces the effect of observation uncertainty by raising the number of independent observations (channels) from two to four, emulating also the channel configuration planned for CoReH2O (Rott et al., 2010).

2.6.2. Nudging Algorithm

Look-up table methods can address some computational challenges in e.g., forward model inversion. However, the season-long lookup tables for perturbed SnowModel runs we applied here at a plot scale, are likely not computationally efficient on larger spatial scales, and have to be constrained temporally, or by precision, when applied over larger geographical areas consisting of more grid cells. This is because they would require numerous SnowModel runs in each grid point.

Alternative, cost efficient solutions were examined based on the findings of the sensitivity experiment. We used a consistent behavior pattern of the microwave-based SWE retrievals to correct the SnowModel SWE by using the SnowModel assimilation scheme (SnowAssim). We created a bias correction nudging algorithm that was implemented in each time step based on the following condition: if at $T = t$ retrieved SWE(t) is greater than the modeled SWE(t) by 5%, then SnowModel SWE(t) is assimilated with SWE'(t) (Equation 10), (nudged by 10%) to the opposite direction:

$$\mathrm{SWE}'(t) = 1.1 \times \mathrm{SWE}(t) \tag{10}$$

The SnowModel run was repeated with assimilation at $T = t$, until the next time step ($T = t + 1$), when the nudging algorithm was applied again. For this study, we implemented the nudging algorithm once every month. However, the time step can be adjusted according to the application's needs.

3. Results

3.1. Comparison of Synthetic (Modeled) to Observed Microwave Observations

We created a set of synthetic microwave observations, by directly inserting simulated snowpack states from SnowModel's base run and SWE-perturbed runs (±50%) into MEMLS (see Figure 1). Figure 3 depicts a comparison between synthetic and real brightness temperatures for vertically polarized channels of 18.7 and 36.5 GHz, for years 2010, 2011, and 2013, at 50° incidence angle. The shaded areas seen in Figures 3 and 4 are created by the perturbed runs at ±50% SWE. Table 2 summarizes the statistics of both active and passive simulations against observed TB and backscatter for the period from January 1 to March 31 of each year. The brightness temperature simulations at 18.7 GHz showed reasonable agreement with the observations for all years with a bias of −4.8, −1.0, and −0.8 K for 2010, 2011, and 2013, respectively. Simulations

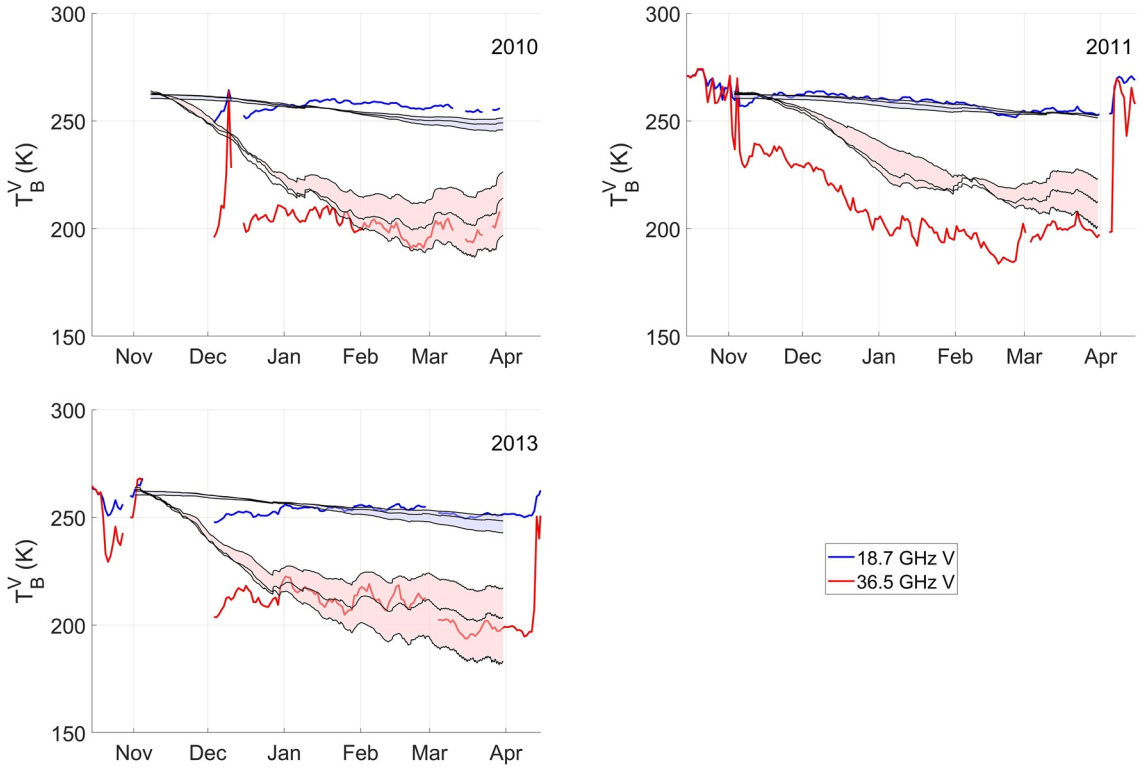

Figure 3. Synthetic (shaded areas) and real (solid lines) observations of V-polarization brightness temperature at 18.7 and 36.5 GHz in 2010 (a), 2011 (b), and 2013 (c).

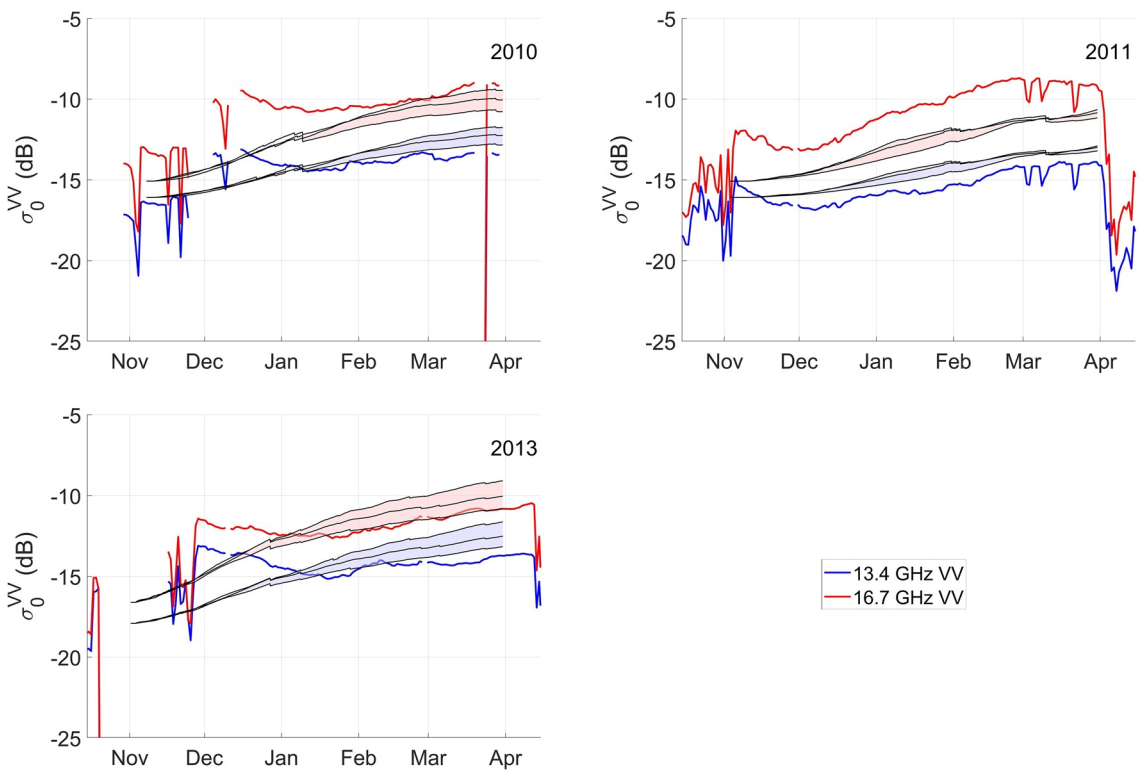

Figure 4. Synthetic (shaded areas) and real (solid lines) observations of VV-polarized backscatter at 13.4 and 16.7 GHz in 2010 (a), 2011 (b), and 2013 (c).

Table 2
Summary of Bias, Unbiased RMS Error, and Coefficient of Determination Between Observed and Modeled Brightness Temperature (K) and Backscatter (dB) for January 1 to March 31 for Years 2010, 2011 and 2013

Passive	Bias (K)		uRMSE (K)		R^2	
Year	18.7 GHz	36.5 GHz	18.7 GHz	36.5 GHz	18.7 GHz	36.5 GHz
2010	−4.8	6.2	1.9	2.9	0.6	0.7
2011	−1.0	21.6	1.3	4.7	0.8	0.3
2013	−0.8	1.3	1.8	4.2	0.5	0.8
Active	Bias (K)		uRMSE (K)		R^2	
Year	13.4 GHz	16.7 GHz	13.4 GHz	16.7 GHz	13.4 GHz	16.7 GHz
2010	0.7	−0.8	0.4	0.4	0.79	0.73
2011	1.1	−2.2	0.3	0.2	0.92	0.91
2013	0.8	0.6	0.5	0.3	0.65	0.84

for 36.5 GHz matched observations closely for 2010 and 2013 (mean absolute error [MAE] less than 6 K), but showed an overestimation for 2011 (bias 22 K). Simulations did not capture the high variability of the 36.5 GHz signal in the early season (note that uninterrupted measurements throughout the winter were available only in 2011). However, for the period of January 1 to March 31, the simulations captured well the general trend of observed TB, as indicated by an (unbiased) RMSE of less than 5 K and R^2 values of over 0.5 for all channels.

Figure 4 depicts a comparison between simulations and observed backscatter at 13.4 and 16.7 GHz, VV polarization, for the same years. Backscattering between January 1 and March 31 is captured well for both frequencies in 2010 and 2013 (bias less than 0.8 dB); simulations for 2011 yield a bias of observed backscatter by 1.1 and −2.2 dB for 13.4 and 16.7 GHz, respectively. As in the case of passive microwaves, the general trend of increasing backscatter in the January 1 to March 31 period is nevertheless well captured, with an (unbiased) RMSE of less than 0.4 dB, and R^2 values of over 0.65 for all channels.

A notable feature in the backscatter simulations was the discrepancy between the observations and the simulations in the early season. The distinct increase in backscatter apparent in December 2009, November 2010, and late November–December 2012 was not repeated by the simulations. This has been attributed to early season crust formation due to melt-refreeze events, causing a source of high backscattering, followed by gradual metamorphism of the crusts evidenced by reduced backscatter (Lemmetyinen et al., 2018; Lin et al., 2016).

The shaded areas depicting the range of simulations obtained with ±50% SWE-perturbed SnowModel runs reveal an overall low sensitivity of TB in February 2011 and backscatter in February–March 2011 to SWE. This is due to the interplay of SnowModel simulated SWE and other snow parameters, in particular correlation length, in the coupled SnowModel-MEMLS system; in these periods, the increase/decrease of SWE in the perturbed runs induces a respective decrease/increase in correlation length, which almost negates the corresponding simulated TB and backscattering response.

3.2. Comparison of SnowModel to in Situ Observations

The use of synthetic microwave observations in this study eliminated the effect of uncertainties in SnowModel and MEMLS predictions. Nevertheless, we compared SnowModel simulations of snow properties to in situ snow profiles to evaluate the overall SnowModel's performance in our study area. SnowModel simulations were performed in a multilayer setup (12 layers). For clarity, snow parameters are presented separately for the top and bottom halves of the snowpack. Figures 5–7 depict modeled and in situ evolution of snow temperature, density, and grain size averaged over the top and bottom halves of the snowpack in 2010, 2011, and 2013. Here, we present the results of the base run.

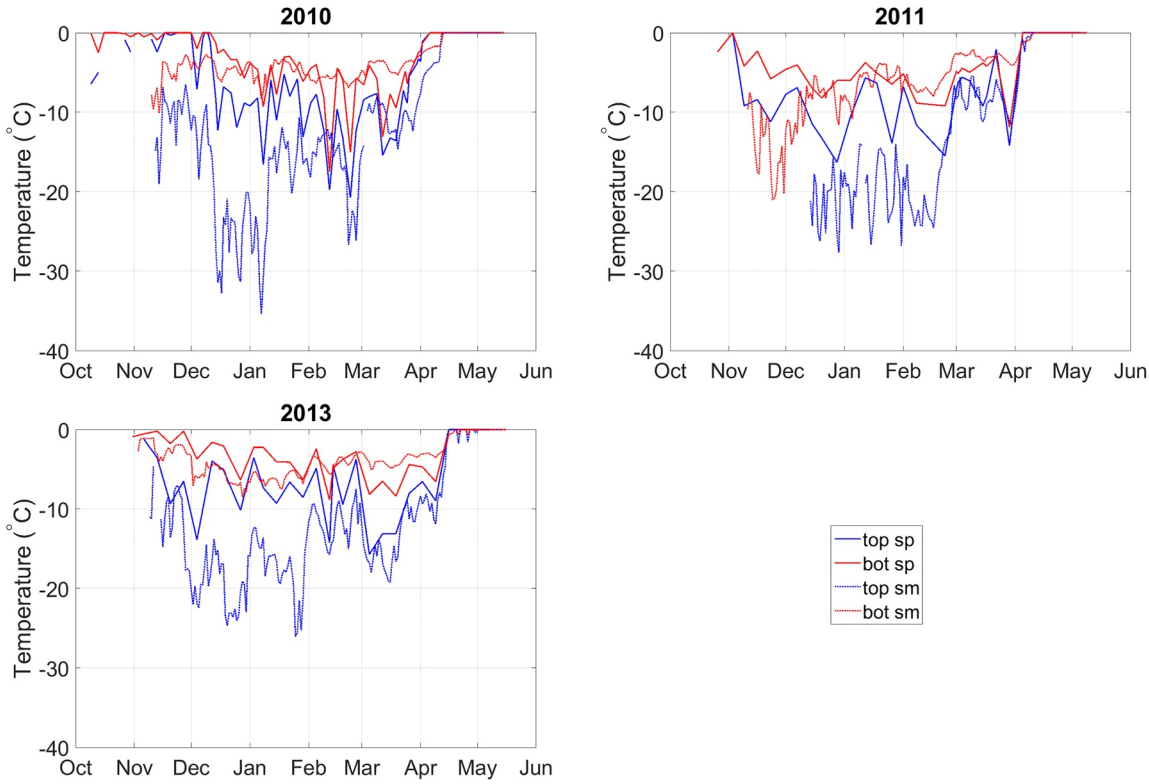

Figure 5. In situ (solid line) and modeled (dashed line) evolution of the snow temperature in 2010 (a), 2011 (b), and 2013 (c). The top (in blue) and the bottom (in red) halves of the snowpack are presented separately. In the legend, sp stands for snow-pit and sm for SnowModel.

Snow temperature was consistently underestimated at the top half of the snowpack, on average by 5°–7°C (Figure 5). The underestimation was especially prominent during the winter months, indicating that low air temperatures modulated faster at the top layers of the snowpack compared to the simulations. SnowModel does not include a canopy downwelling longwave radiation term. This, in combination with the low wind speeds found near the snow surface around forest canopies, means the surface energy budget produces unrealistically low surface temperatures, resulting in cooler top layers of the snowpack. A downwelling canopy radiation term will be added to SnowModel's surface energy balance in the next code update. At the bottom half of the snowpack temperature was mildly underestimated, on average by 0.3°–1.5°C. Snow density was commonly underestimated at the top (on average by 18%) and overestimated at the bottom half of the snowpack (on average by 31%), with large annual variations (Figure 6). The density underestimation at the top is associated with temperature underestimations. The snow densification rate of the bottom layers was higher in the simulations compared to the observations. One reason is that, currently, SnowModel does not account for the effects of snow microstructure to snow density. Snow density is affected by snow microstructure, because the latter affects the snow compaction rate. As an example, in cold snow climates, depth hoar formation at the bottom of the snowpack changes the mechanical properties of the snow, and imposes resistance to densification. The ability to transport mass from one layer of the snowpack to another layer, will be implemented in the next SnowModel code update. Finally, and most importantly, grain size simulations matched exceptionally well to the in situ observations (Figure 7). The mean average bias was at 3%.

3.3. The Sensitivity Experiment

Figure 8 depicts the results of the sensitivity experiment. Retrievals using synthetic observations were performed by assuming snow depth as a free parameter ($\sigma_\alpha \gg 1$ in Equation 3), and fixing all other model parameters, including the microstructure (l_{exp}), to the SnowModel run ($\sigma_\beta \ll 1$ in Equation 3). Retrievals based on the perturbed runs at ±30% are depicted; also depicted are the SWE evolution based on the base

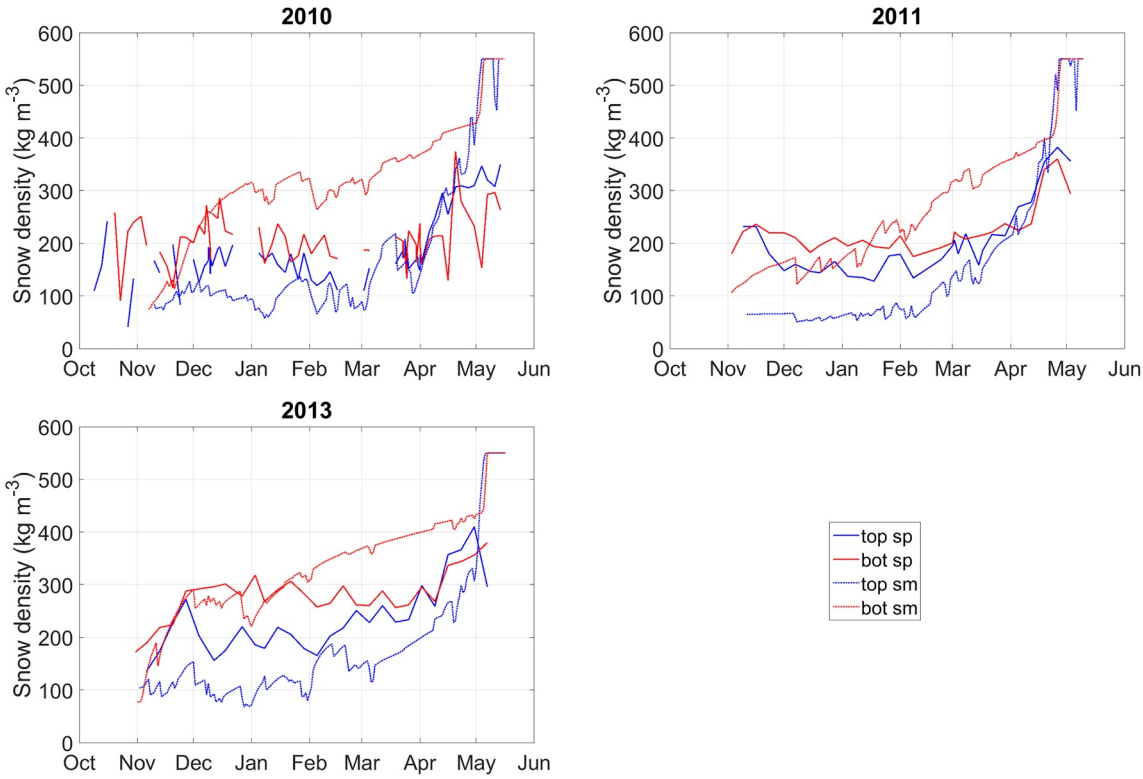

Figure 6. Same as Figure 5 but for snow density.

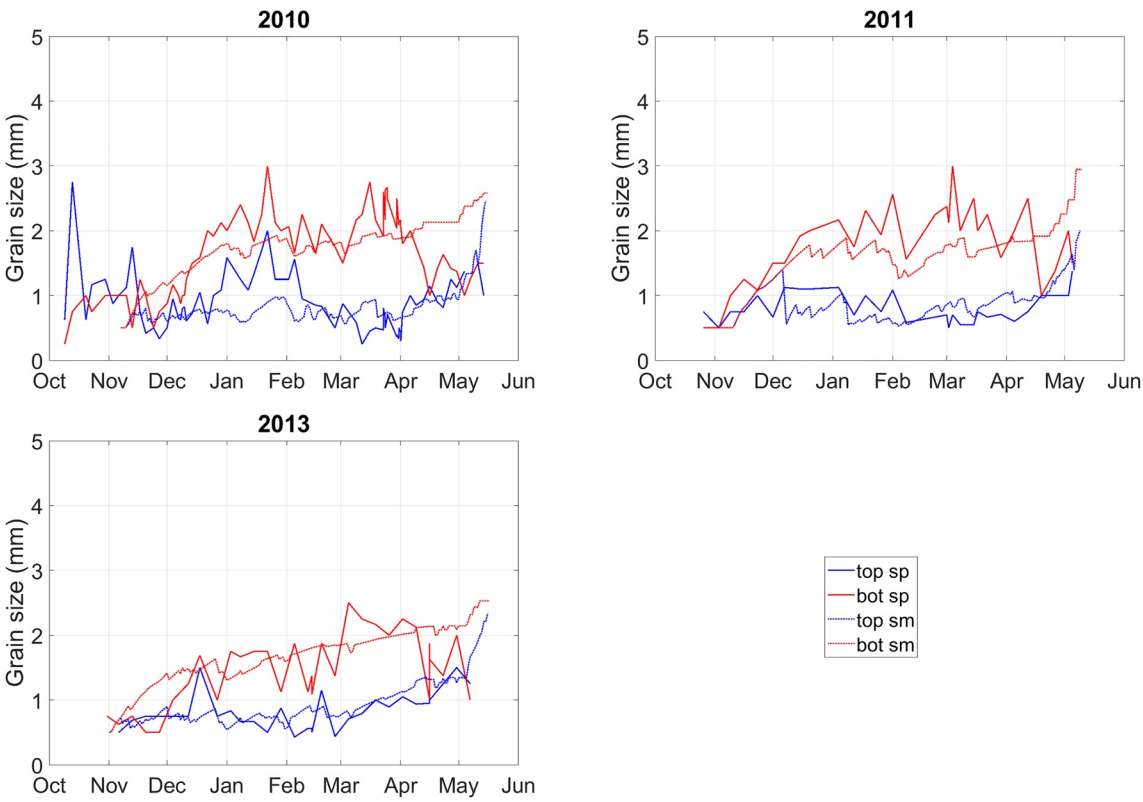

Figure 7. Same as Figure 5 but for snow grain size.

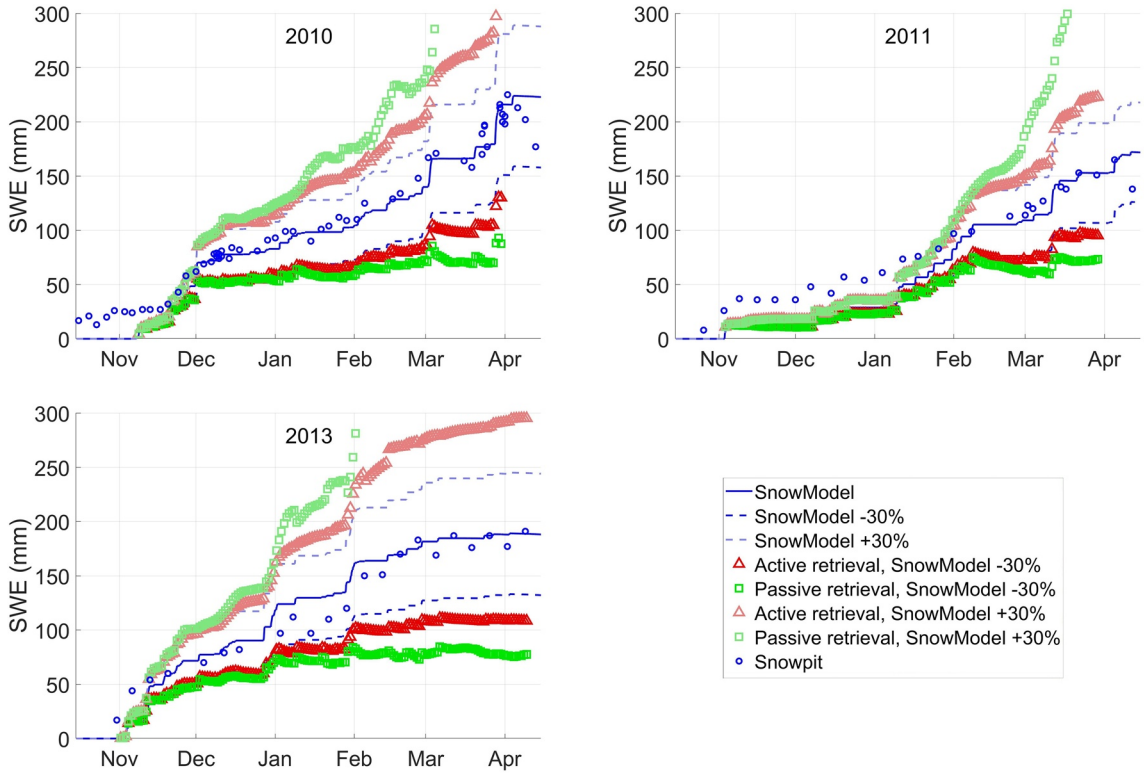

Figure 8. Retrievals of SWE using synthetic active (red triangles) and passive (green squares) microwave observations, using snowpack states from ±30% SWE perturbed runs. Modeled SWE from the base run (blue line) and from the SWE-perturbed runs (dashed blue lines) are shown together with in situ measured SWE (blue squares) in 2010 (a), 2011 (b), and 2013 (c).

run and on the SWE-perturbed runs (±30%). Total SWE measured from weekly (2011, 2013) and bi-weekly (2010) snow-pits is also shown.

When utilizing snowpack states from SWE-perturbed SnowModel runs, and fixing all parameters - except snow depth - in the cost function, the microwave-based SWE retrievals were pulled away from valid solutions (Figure 8). The reason is that in physical snow models, as in nature, SWE is inversely related to grain size. This happens because metamorphic grain growth is directly related to temperature gradients within the snowpack. In thicker snowpacks, temperature gradients are dampened, and so does the grain growth rate of the snowpack. Thus, if SWE is overestimated, average grain size will be underestimated as a response, and vice versa. In microwave models however, SWE and grain size are both directly, not inversely, related to the microwave signatures (e.g., simulated backscatter increases both with increase of SWE and increase of grain size/correlation length). In addition, scattering of microwaves is very sensitive to the snow microstructure. Therefore, natural changes of grain size that correspond to changes in SWE, dictate the simulations of microwave signatures. When the cost function is fixed to a biased grain size, and does not account for the natural relationship between SWE and grain size, it adjusts SWE in the wrong direction in order to match the observation, resulting in additional deterioration of the retrieval. This pattern was consistent in all years, even for small changes in the modeled SWE (±10%). The problem can in some cases be alleviated by adjusting factors σ_α and σ_β to enable an actual two-parameter retrieval, where both SWE and microstructure are fluctuated in the minimization of the cost function; here, the microstructure was fixed in order to demonstrate the full impact of the inverse relation of magnitude of SWE and microstructure in the SnowModel outputs.

Figure 9 depicts the MAE of SWE between in situ observations, SnowModel runs and SWE retrievals based on these runs. The MAE of both active and passive SWE retrievals is always larger when compared to the MAE of the SWE-perturbed SnowModel runs. MAE of active retrievals is 17%–82% larger than the MAE of the SWE-perturbed runs. MAE of passive retrievals is 58%–293% larger than the MAE of the SWE-perturbed

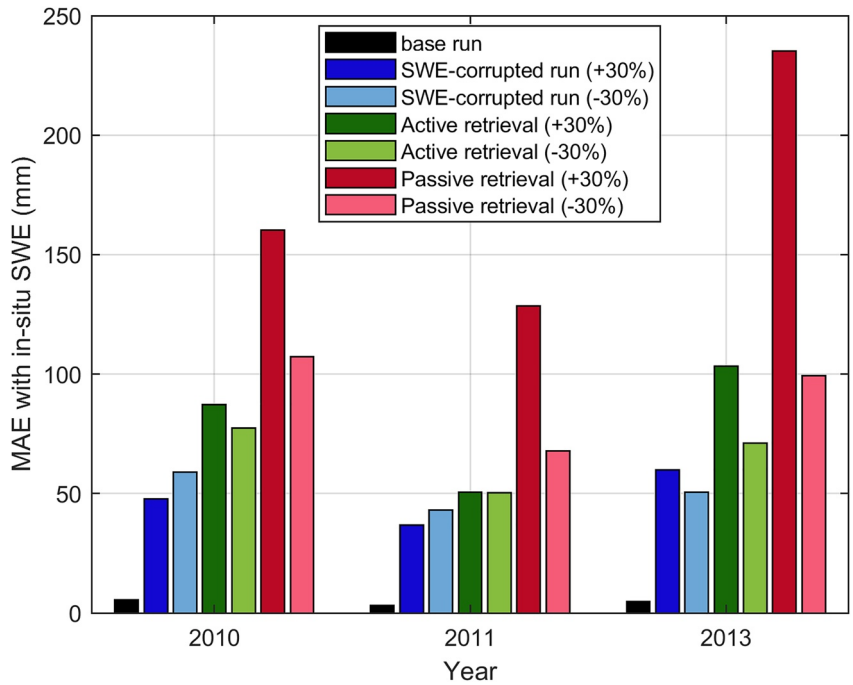

Figure 9. MAE between in situ SWE in March and SnowModel base run (black), SnowModel SWE-perturbed runs ±30% (blue), passive (red) and active (green) retrievals based on the SWE-perturbed runs in 2010, 2011, and 2013.

runs. We noticed that passive retrievals produced larger biases compared to active retrievals. Also, biases are 2–3 times larger when retrievals are guided by runs that overestimate SWE compared to SWE runs that underestimate SWE.

3.4. SWE Retrievals Using Look-Up Tables

Results from the sensitivity experiment indicated that even for small biases in modeled SWE (±10%), the corresponding changes in microstructure typically increased the biases in SWE retrievals from microwave signatures. To overcome this challenge, the natural relationship between SWE and microstructure needs to be considered in SWE retrieval algorithms. One way is to provide the cost function with a set of look-up tables: physically simulated groups of all snowpack states. In that manner, SWE and microstructure would not be used as minimization parameters independently from one another, and consequently errors related to their natural dependence would be mitigated.

Following the method described in Section 2.6, we examined the distribution of bias in SWE retrievals for different levels of noise in the synthetic observations. As an example, histograms in Figures 10 and 11 depict the distributions on 30 March for each year for passive and active microwave retrievals, respectively. Deviation from the SnowModel base run is depicted as the likelihood of deviation in %, binned in 5% categories. The depicted SWE biases are characterized by normal distributions. It is evident however that when noise levels increase, the bell curves flatten, increasing the uncertainty of SWE retrievals.

The average standard deviation of the SWE retrievals was calculated every year for March (Table 3). Based on the standard deviations, SWE uncertainties ranged from 6% to 36% in passive, and from 8% to 43% in active depending on the noise levels. The largest sensitivity to observation uncertainty is apparent for active microwave retrievals in 2011, where already modest uncertainty of 0.4 dB leads to a large part of retrievals being outside a ±50% uncertainty range. This is due to the low overall sensitivity of the coupled model to SWE for this particular season, already apparent in forward model simulations (see Section 3.1).

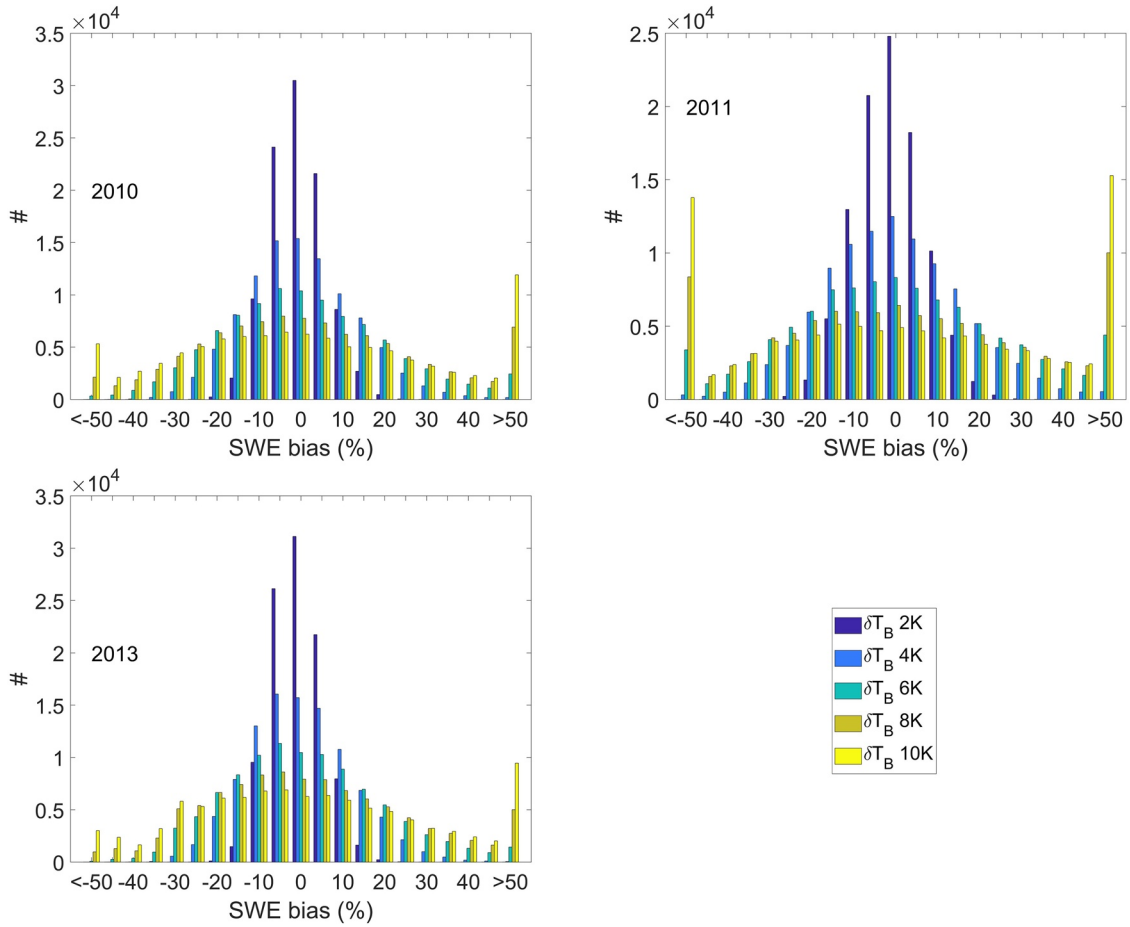

Figure 10. Distribution of SWE bias (%) in passive microwave retrievals on 30 March based on the look-up table method. Different bar colors correspond to different noise levels ranging from 2 to 10 K.

3.5. SWE Retrievals Using a Nudging Algorithm

We used the SWE-perturbed runs of ±30% for testing the nudging algorithm described in Section 2.6. The nudging algorithm was implemented once a month to assimilate the SnowModel with microwave signatures, based on the condition that even small biases in modeled SWE pull the retrievals away from valid SWE solutions. The results are depicted in Figures 12 and 13, and they correspond to SnowModel SWE underestimation (−30%) and overestimation (+30%) respectively. Results are presented from the perspective of SnowModel. The time steps when the nudging algorithm was implemented (first day of each month) are indicated in both figures.

Implementing the bias correction nudging algorithm once a month substantially improved the SWE-perturbed SnowModel runs (Figures 12 and 13). Green and red lines correspond to SnowModel runs with SWE assimilation based on the utilization of passive and active retrievals respectively. This approach is cost efficient for large scale applications, and worthy of further investigation. Possible limitations of this method are related to the impact of changes in SWE to the snow microstructure. We hypothesize that in milder snow climates changes in SWE will have a smaller impact on the grain growth rate, and potentially invalidate the condition we apply here. To investigate that, we created an artificial meteorological data set where we kept air temperature at −1°C during the snow season, to maintain mild temperature gradients inside the snowpack. We found again that small changes in the modeled SWE consistently pulled the retrieval away from a valid solution (not shown). Therefore, the condition for applying the bias correction nudging algorithm is valid also in milder snow climates.

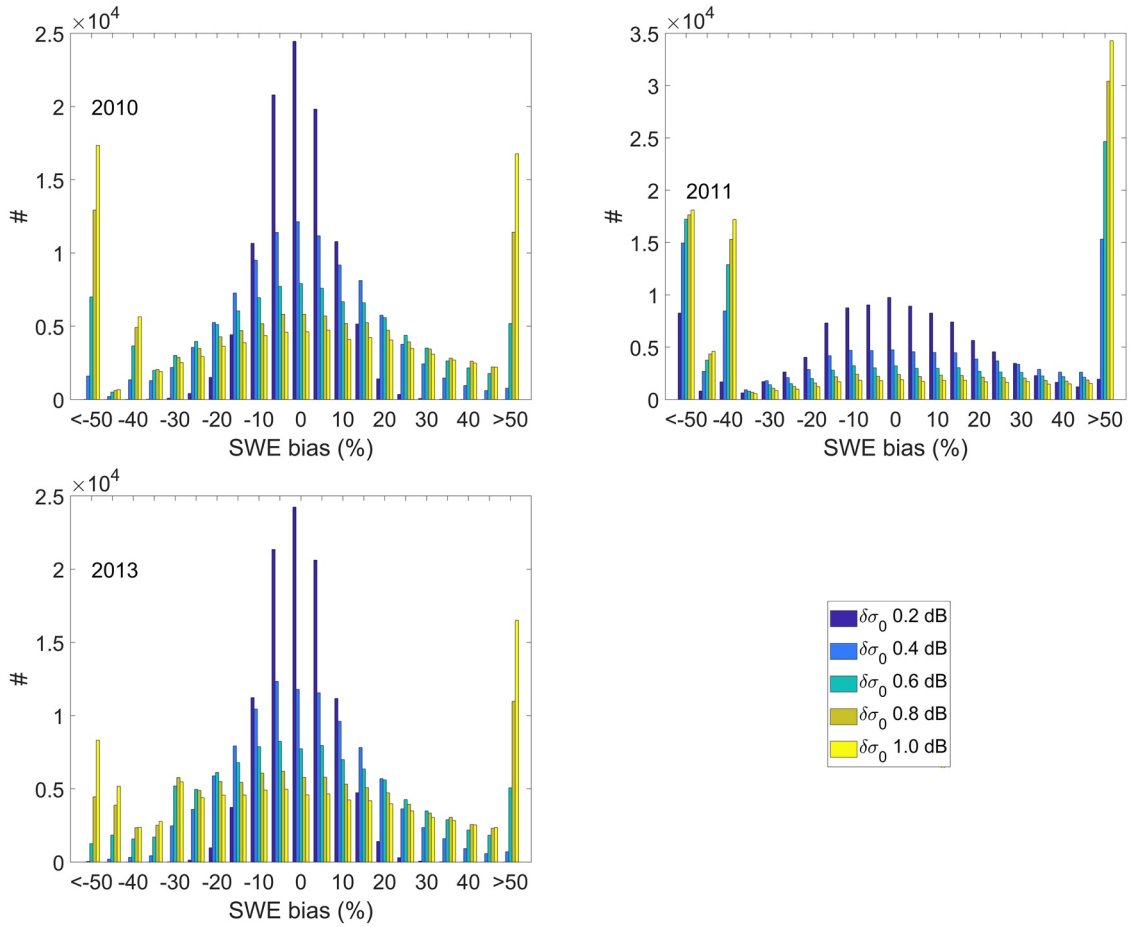

Figure 11. Distribution of SWE bias (%) in active microwave retrievals on 30 March based on the look-up table method. Different bar colors correspond to different noise levels ranging from 0.2 to 1 dB.

4. Discussion

Microwave signatures are strongly affected by several snowpack states, but most critically by snow microstructure. Currently, information on snowpack states is either derived by interpolating sparse in situ observations (Takala et al., 2011), or simplified grain growth models (Kelly et al., 2003). Utilizing snowpack states from physical snow models is—in theory—an ideal way to improve SWE retrievals from microwaves. The main challenge is related to uncertainties in modeled SWE that often derive from uncertainties in the

Table 3
Mean Standard Deviation (% of SWE) of March Retrievals From Active and Passive Microwaves

Year/noise level	δTB 2K	δTB 4K	δTB 6K	δTB 8K	δTB 10K
2010	7	14	21	27	31
2011	11	21	28	33	36
2013	6	13	19	24	28
	δσ0 0.2 dB	δσ0 0.4 dB	δσ0 0.6 dB	δσ0 0.8 dB	δσ0 1 dB
2010	8	18	27	32	35
2011	24	35	39	41	43
2013	8	17	24	29	33

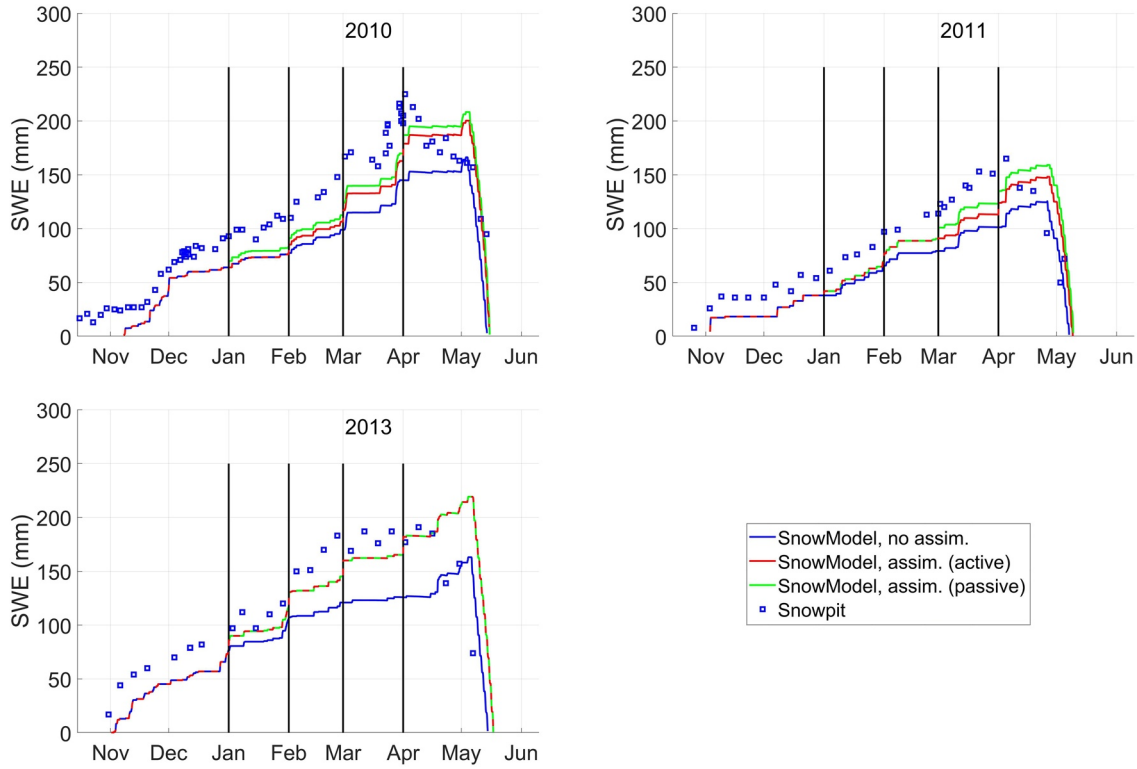

Figure 12. SWE-perturbed SnowModel runs (−30% end-of-season SWE) (blue line), and SnowModel runs corrected by the nudging algorithm guided by active (red line) and passive (green line) microwave observations. In situ measured SWE (blue squares), and dates of implementing the nudging algorithm (black lines) in years 2010 (a), 2011 (b), and 2013 (c) are indicated.

precipitation forcing. Uncertainties in modeled SWE consequently affect several other snow properties, in particular the snow microstructure.

We chose SnowModel as the physical model because it can evolve snow distributions using grid increments from 1 m to tens of km, over a wide range of spatial and temporal domains. SnowModel has been widely tested in environments where snow can occur, including glaciers and sea ice. Therefore, it is potentially an ideal candidate for upscaling the methods to satellite/global scales. The size and the seasonal evolution of snow microstructure, the most critical parameter in microwave models, was captured remarkably well by SnowModel.

We used MEMLS to simulate passive and active microwave signatures, using the information of snowpack states from SnowModel, as MEMLS offers a unified physical approach for simulating both active and passive microwave signatures with a relatively small number of tuning parameters. The uncertainty of MEMLS in studies applying snowpit data to generate microwave observables has been reported as e.g., 7–11 K RMSE for brightness temperature at 7–37 GHz (Pan et al., 2015). On the other hand, when using snow-pit data with microstructure first optimized using passive observations, Lemmetyinen et al. (2016) reported an unbiased RMSE between 0.6 and 1.0 dB for backscatter at 10.2 and 16.7 GHz (VV polarization).

A sensitivity experiment quantified the effects of uncertainty in physically simulated SWE to the SWE retrievals from microwave signatures, due to the consequent effects in the rest of the snowpack states, especially in the snow microstructure. Synthetic observations generated using the coupled SnowModel-MEMLS system, were used instead of real ones, in order to remove random uncertainties related to microwave observations. Although simulations with the coupled model indicated a reasonable match with observed brightness temperature and backscatter (Figures 3 and 4), real microwave observations introduced a random element that varied from year to year. Consequently, when real observations were applied, unambiguous interpretation of the sensitivity test in Section 3.3 was challenging; in some years retrievals with SWE-perturbed SnowModel runs were seemingly close to the in situ measured SWE - this was, however,

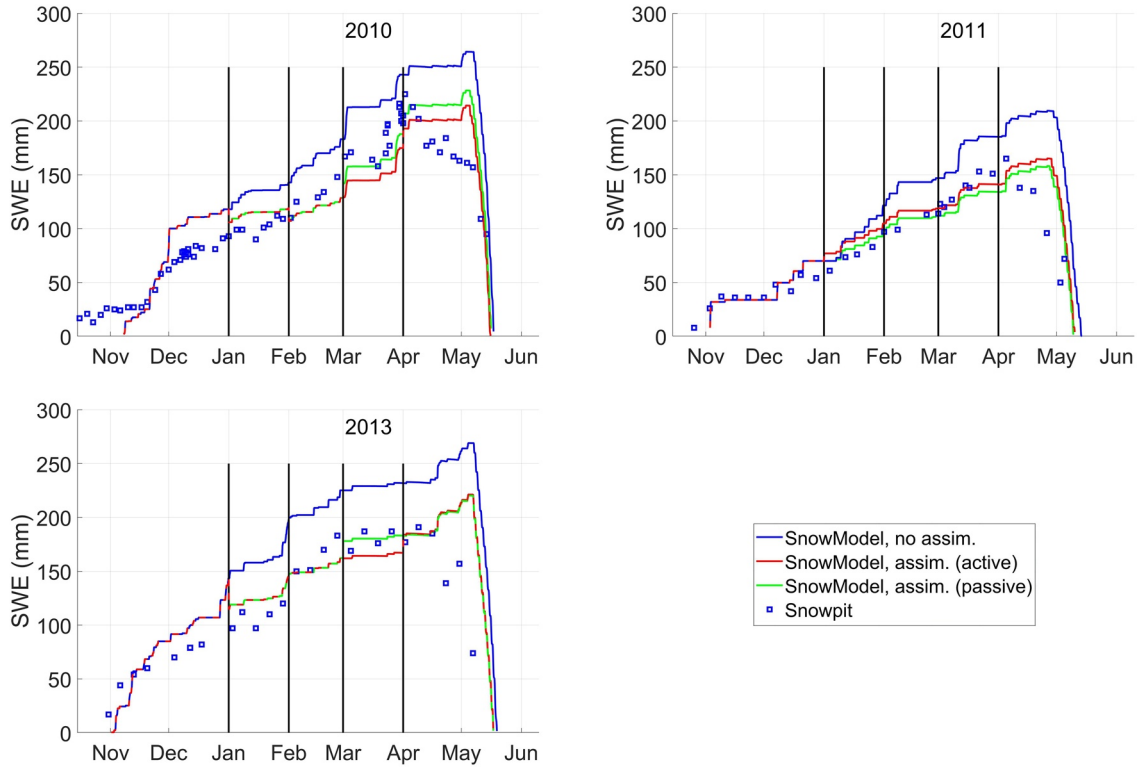

Figure 13. Same as Figure 12 but for SnowModel run perturbed by +30% end-of-season SWE.

incidental and due to e.g., the simulations for that year under- or overestimating the observed signal. We thus chose to use the synthetic observations, which removed this random element, and demonstrated the impact of SnowModel-simulated SWE and microstructure on microwave retrievals in a more controlled simulation environment. Tests with a large number of cases of real observations are nevertheless expected to yield similar results regarding sensitivity to SWE and microstructure, providing that the coupled model simulations are not severely unbiased compared to observations.

A look-up table approach was examined to address the challenges identified by the sensitivity experiment. In this study, the demonstration was simplified. The retrieval algorithm was fixed to predefined groups of SWE and snowpack states to preserve their natural relationship. However, there was no freedom for adjustments; when the look-up table combinations were applied strictly, they provided a narrow range of solutions available for the retrieval algorithm to implement. The range was narrow due to the inverse relationship of SWE and average grain size of the snowpack that canceled out their relative effect in microwave models, causing small changes in the simulated microwave signatures. This is demonstrated clearly in Figure 3b, where the real observations are outside the range of synthetic observations that were produced from ±50% SWE-perturbed runs. In practical applications, adjustments can be induced by allowing a degree of freedom to the implemented snow states, e.g., by adjusting the variances of reference values ($\sigma_{\alpha,\mathrm{ref}}$ and $\sigma_{\beta,\mathrm{ref}}$ in Equation 3). The final outcome of the retrieval can also be a combination of the original SnowModel run and the assimilation retrieval, placing a degree of confidence on both.

Finally, a nudging algorithm was examined to investigate a significantly more cost efficient method compared to the look-up tables. Cost efficient methods are necessary for large scale SWE retrieval applications. The results of the nudging algorithm looked promising, managing to improve substantially modeled biases in SWE. This method is worthy of further investigation related to its applicability in different snow climates.

5. Conclusions

In this study, we identified challenges related to uncertainties in SWE simulations, when assimilating microwave signatures with physical snow models. We performed a sensitivity experiment over a small area in northern Finland, where a data set of in situ, passive and active microwave observations of snow cover was available in 2010, 2011, and 2013. We perturbed the simulated SWE in a controlled manner, to examine how biases in modeled SWE affect the rest of the snowpack states and, consequently, the microwave-based SWE retrievals. To achieve that we emulated a method used previously in microwave-based SWE retrievals: setting snow depth as a free parameter, and fixing all other parameters, including the microstructure, to the SWE-perturbed SnowModel runs.

The sensitivity experiment revealed a consistent deterioration of the microwave-based SWE retrievals when driven by SWE-perturbed simulations. The deterioration occurred even for small SWE perturbations (±10%), exhibiting a critical challenge when assimilating microwave signatures with physical snow models. In simple words, biases in the physically modeled SWE would induce even larger biases in microwave-based SWE retrievals, by introducing an increasingly biased estimate of snow microstructure to the retrieval. Microwave-based SWE retrievals guided by ±30% SWE-perturbed simulations, had up to 3 times larger end-of-season MAE compared to the MAE of the SWE-perturbed simulations themselves. Specifically, MAE increased by up to 82% in active and 293% in passive microwaves. MAE of the retrievals was 2–3 times larger when SWE was overestimated by the SnowModel. Past studies (e.g., Kontu et al., 2017; Langlois et al., 2012; Sandells et al., 2017) have analyzed the capability of physical snow models to produce snow microstructure estimates required by the microwave-based SWE retrievals, when models are driven by ideal data producing a SWE close to reality. This study examined the impact of microstructure estimates produced under biased estimates of SWE, to address more realistic, practical applications.

To overcome this challenge, the retrieval algorithm needs to account for the natural relationship between SWE and snow microstructure. We created annual look-up tables with time series of snowpack states provided by a set of SWE-perturbed SnowModel runs. We guided the retrieval algorithm to look for solutions directly from the look-up tables. This way the solutions corresponded to combinations of the snowpack states with respect to their natural relationship. We induced noise in the synthetic observations to examine the effect of observation uncertainties. The increase in noise levels increased the uncertainty of the retrievals. Uncertainty of passive retrievals ranged from 6% for 2 K noise levels to 36% for 10 K noise levels. In active retrievals, uncertainty ranged from 8% for 0.2 dB noise levels to 43% for 1 dB noise levels.

For practical applications, a more cost-efficient assimilation method was examined. A bias correction nudging algorithm was implemented once a month to assimilate the SnowModel with microwave signatures, based on the condition that even small biases in modeled SWE pull the retrievals away from valid SWE solutions. This method demonstrated a strong potential to improve SnowModel simulations by correcting biases in SWE simulations, often originating from precipitation biases. More sophisticated approaches could involve utilization of physical snow models to establish simplified functions between SWE and snow microstructure, based on snow aging. More research is required to create a cost-efficient automated synergetic system between physical and microwave models for application on satellite scales, as well as the applicability of other microwave forward models and physical snow models for the purpose.

A system where both physical models and microwave signatures work in synergy can benefit snow remote sensing. Our results demonstrate that assimilating microwave signatures with physical snow models face critical challenges, associated with the different nature in the relations between SWE and snow microstructure in these models. However, when the microwave-based SWE retrieval algorithms account for these relationships, there is good potential for improving SWE retrievals via synergies. To conclude, this study suggests that physical models with the ability to simulate realistic relationships between the snowpack properties required for the microwave-based SWE retrievals, such as SnowModel, can be valuable candidates for SWE retrieval applications.

Data Availability Statement

NoSREx data are publicly available at the ESA campaign data portal (https://earth.esa.int/web/guest/pi-community/apply-for-data/campaigns). Weather station data in Sodankylä are available at https://litdb.fmi.fi/luo0015_data.php.

Acknowledgments
The work was funded by the Academy of Finland Research Fellowship grant "Advanced Satellite Techniques and Retrieval Algorithms for detecting seasonal snow mass" (325397). It was additionally supported by National Aeronautics and Space Administration grant 80NSSC18K0571. The NoSREx campaign was funded by the European Space Agency (Contract No. 22671/09/NL/JA). The authors warmly thank the NoSREx campaign team responsible for collecting and post-processing the snow-pit data. Finally, the authors would like to thank Prof. Michael Durand for his constructive and helpful comments on this study.

References

Aas, K. S., Gisnås, K., Westermann, S., & Berntsen, T. K. (2017). A tiling approach to represent subgrid snow variability in coupled land surface-atmosphere models. *Journal of Hydrometeorology*, *18*, 49–63. https://doi.org/10.1175/JHM-D-16-0026.1

Anderson, E. A. (1976). *A point energy and mass balance model of a snow cover*. NOAA Technical Report.

Barnett, T., Adam, J., & Lettenmaier, D. (2005). Potential impacts of a warming climate on water availability in snow-dominated regions. *Nature*, *438*, 303–309. https://doi.org/10.1038/nature04141

Boisvert, L. N., Webster, M. A., Petty, A. A., Markus, T., Bromwich, D. H., & Cullather, R. I. (2018). Intercomparison of precipitation estimates over the Arctic ocean and its peripheral seas from reanalyses. *Journal of Climate*, *31*(20), 8441–8462. https://doi.org/10.1175/JCLI-D-18-0125.1

Brown, R. D., & Mote, P. W. (2009). The response of Northern hemisphere snow cover to a changing climate. *Journal of Climate*, *22*(8), 2124–2145. https://doi.org/10.1175/2008JCLI2665.1

Brun, E., Vionnet, V., Boone, A., Decharme, B., Peings, Y., Valette, R., et al. (2013). Simulation of northern Eurasian local snow depth, mass, and density using a detailed snowpack model and meteorological reanalyses. *Journal of Hydrometeorology*, *14*(1), 203–219. https://doi.org/10.1175/JHM-D-12-012.1

Colbeck, S. C. (1990). *The international classification for seasonal snow on the ground*. International Commission on Snow and Ice, International Association of Scientific Hydrology.

Dai, L. Y., Che, T., Wang, J., & Zhang, P. (2012). Snow depth and snow water equivalent estimation from AMSR-E data based on a priori snow characteristics in Xinjiang, China. *Remote Sensing of Environment*, *127*, 14–29. https://doi.org/10.1016/j.rse.2011.08.029

Davenport, I. J., Sandells, M. J., & Gurney, R. J. (2012). The effects of variation in snow properties on passive microwave snow mass estimation. *Remote Sensing of Environment*, *118*, 168–175. https://doi.org/10.1016/j.rse.2011.11.014

De Lannoy, G. J. M., Reichle, R. H., Houser, P. R., Arsenault, K. R., Verhoest, N. E. C., & Pauwels, V. R. N. (2010). Satellite-ssale snow water equivalent assimilation into a high-resolution land surface model. *Journal of Hydrometeorology*, *11*(2), 352–369. https://doi.org/10.1175/2009jhm1192.1

Derksen, C., Lemmetyinen, J., King, J., Belair, S., Garnaud, C., Lapointe, M., et al. (2019). A dual-frequency Ku-band radar mission concept for seasonal snow. In *IGARSS 2019—2019 IEEE International Geoscience and Remote Sensing Symposium* (pp. 5742–5744). https://doi.org/10.1109/IGARSS.2019.8898030

Durand, M., Kim, E. J., & Marguilis, S. (2009). Radiance assimilation shows promise for snowpack characterization. *Geophysical Research Letters*, *36*(2), a–n. https://doi.org/10.1029/2008GL035214

Durand, M., & Liu, D. (2012). The need for prior information in characterizing snow water equivalent from microwave brightness temperatures. *Remote Sensing of Environment*, *126*, 248–257. https://doi.org/10.1016/j.rse.2011.10.015

Essery, R. L. H., Kontu, A., Lemmetyinen, J., Dumond, M., & Menard, C. B. (2016). A 7 yr data set for driving and evaluating snow models at an Arctic site (Sodankylä, Finland). *Geoscientific Instrumentation, Methods and Data Systems*, *5*, 219–227. https://doi.org/10.5194/gi-5-219-2016

Fierz, C., Armstrong, R. L., Durand, Y., Etchevers, P., Greene, E. M., Mcclung, D. M., et al. (2009), *The International Classification for Seasonal Snow on the Ground. (IHP Technical Documents in Hydrology 83)*. UNESCO-International Hydrological Programme.

Foster, J. L., Liston, G. E., Essery, R., Behr, H., Dumenil, L., Verseghy, D., et al. (1994). Intercomparison of snow cover and snow mass in North America from general circulation models and remote sensing. In *American Meteorological Society. Sixth Conference on Climatic Variation, Nashville, Tennessee* (pp. 207–211). American Meteorological Society.

Gonzalez, R., & Kummerow, C. D. (2020). AMSR-E snow: Can snowfall help improve SWE estimates? *Journal of Hydrometeorology*, *21*(11), 2551–2564. https://doi.org/10.1175/JHM-D-20-0066.1

Jordan, R. (1991). *A one-dimensional temperature model for snow cover. Technical documentation for SNTHERM* (Vol. 89). US Army Corps of Engineers.

Kelly, R., Chang, A., Tsang, L., & Foster, J. (2003). A prototype AMSR-E global snow area and snow depth algorithm. *IEEE Transactions on Geoscience and Remote Sensing*, *41*(2), 230–242. https://doi.org/10.1109/tgrs.2003.809118

Kojima, K. (1967). Densification of seasonal snow cover. In H. Ôura (Ed.), *Physics of snow and ice* (Vol. 1, pp. 929–952). Institute of Low Temperature Science, Hokkaido University.

Kontu, A., Lemmetyinen, J., Vehviläinen, J., Leppänen, L., & Pulliainen, J. (2017). Coupling SNOWPACK-modeled grain size parameters with the HUT snow emission model. *Remote Sensing of Environment*, *194*, 33–47. https://doi.org/10.1016/j.rse.2016.12.021

Langlois, A., Royer, A., Derksen, C., Montpetit, B., Dupont, F., & Goita, K. (2012). Coupling the snow thermodynamic model SNOWPACK with the microwave emission model of layered snowpacks for subarctic and arctic snow water equivalent retrievals. *Water Resources Research*, *48*, W12524. https://doi.org/10.1029/2012wr012133

Larue, F., Royer, A., De Sève, D., Langlois, A., Roy, A., & Brucker, L. (2016). Validation analysis of the GlobSnow-2 database over an eco-climatic latitudinal gradient in Eastern Canada. *Remote Sensing of Environment*, *194*, 264–277.

Lemmetyinen, J., Derksen, C., Rott, H., Macelloni, G., King, J., Schneebeli, M., et al. (2018). Retrieval of effective correlation length and snow water equivalent from active and passive microwave observations. *Remote Sensing*, *10*, 170. https://doi.org/10.3390/rs10020170

Lemmetyinen, J., Kontu, A., Pulliainen, J., Vehviläinen, J., Rautiainen, K., Wiesmann, A., et al. (2016). Nordic snow radar experiment. *Geoscientific Instrumentation, Methods, and Data Systems*, *5*, 403–415. https://doi.org/10.5194/gi-5-403-2016

Leppänen, L., Kontu, A., Hannula, H.-R., Sjöblom, H., & Pulliainen, J. (2016). Sodankylä manual snow survey program. *Geoscientific Instrumentation, Methods, and Data Systems*, *5*, 163–179. https://doi.org/10.5194/gi-5-163-2016

Leppänen, L., Kontu, A., Vehviläinen, J., Lemmetyinen, J., & Pulliainen, J. (2015). Comparison of traditional and optical grain-size field measurements with SNOWPACK simulations in a taiga snowpack. *Journal of Glaciology*, *61*, 151–162. https://doi.org/10.3189/2015jog14j026

Li, W., Guo, W., Qiu, B., Xue, Y., Hsu, P.-C., & Wei, J. (2018). Influence of Tibetan Plateau snow cover on East Asian atmospheric circulation at medium-range time scales. *Nature Communications*, *9*, 1–9. https://doi.org/10.1038/s41467-018-06762-5

Lin, C., Rommen, B., Floury, N., Schuttemeyer, D., Davidson, M. W., Kern, M., et al. (2016). Active microwave scattering signature of snowpack-continuous multiyear SnowScat observation experiments. *IEEE Journal of Selected Topics in Applied Earth Observations and Remote Sensing*, *9*, 3849–3869. https://doi.org/10.1109/JSTARS.2016.2560168

Lindsay, R., Wensnahan, M., Schweiger, A., & Zhang, J. (2014). Evaluation of seven different atmospheric reanalysis products in the arctic. *Journal of Climate*, *27*(7), 2588–2606. https://doi.org/10.1175/JCLI-D-13-0001410.1175/jcli-d-13-00014.1

Liston, G. E., & Elder, K. (2006a). A distributed snow-evolution modeling system (SnowModel). *Journal of Hydrometeorology*, *7*, 1259–1276. https://doi.org/10.1175/jhm548.1

Liston, G. E., & Elder, K. (2006b). A meteorological distribution system for high-resolution terrestrial modeling (MicroMet). *Journal of Hydrometeorology*, *7*, 217–234. https://doi.org/10.1175/jhm486.1

Liston, G. E., Haehnel, R. B., Sturm, M., Hiemstra, C. A., Berezovskaya, S., & Tabler, R. D. (2007). Simulating complex snow distributions in windy environments using SnowTran-3D. *Journal of Glaciology*, *54*, 241–256. https://doi.org/10.3189/172756507782202865

Liston, G. E., & Hall, D. K. (1995). An energy balance model of lake ice evolution. *Journal of Glaciology*, *41*, 373–382. https://doi.org/10.1017/s0022143000016245

Liston, G. E., & Hiemstra, C. A. (2008). A simple data assimilation scheme for complex snow distributions (SnowAssim). *Journal of Hydrometeorology*, *9*, 989–1004. https://doi.org/10.1175/2008jhm871.1

Liston, G. E., & Hiemstra, C. A. (2011). The changing cryosphere: Pan-Arctic snow trends (1979–2009). *Journal of Climate*, *24*(21), 5691–5712. https://doi.org/10.1175/jcli-d-11-00081.1

Liston, G. E., Itkin, P., Stroeve, J., Tschudi, M., Stewart, J. S., Pedersen, S. H., et al. (2020). A Lagrangian snow-evolution system for sea-ice applications (SnowModel-LG): Part I-model sescription. *Journal of Geophysical Research: Oceans*, *125*(10). https://doi.org/10.1029/2019JC015913

Liston, G. E., & Mernild, S. H. (2012). Greenland freshwater runoff. Part I: A runoff routing model for glaciated and nonglaciated landscapes (HydroFlow). *Journal of Climate*, *25*, 5997–6014. https://doi.org/10.1175/jcli-d-11-00591.1

Liston, G. E., & Sturm, M. (1998). A snow-transport model for complex terrain. *Journal of Glaciology*, *44*, 498–516. https://doi.org/10.3189/s0022143000002021

Maggioni, V., Meyers, P. C., & Robinson, M. D. (2016). A review of merged high-resolution satellite precipitation product accuracy during the Tropical Rainfall Measuring Mission (TRMM) Era. *Journal of Hydrometeorology*, *17*, 1101–1117. https://doi.org/10.1175/JHM-D-15-0190.1

Mätzler, C., & Wiesmann, A. (1999). Extension of the microwave emission model of layered snowpacks to coarse-grained snow. *Remote Sensing of Environment*, *70*(3), 317–325. https://doi.org/10.1016/s0034-4257(99)00047-4

Merkouriadi, I., Leppäranta, M., & Järvinen, O. (2017). Interannual variability and trends in winter weather and snow conditions in Finnish Lapland. *Estonian Journal of Earth Sciences*, *66*(1), 4757. https://doi.org/10.3176/earth.2017.03

Météo France. (1996). *The snow cover model CROCUS, technical description, version 2.2. Saint-fMartin-d'Hères Cedex, CNRM/CEN*. Centre National du Machinisme Agricole du Génie Rural, des Eaux et des Forêts.

Mudryk, L. R., Kushner, P. J., Derksen, C., & Thackeray, C. (2017). Snow cover response to temperature in observational and climate model ensembles. *Geophysical Research Letters*, *44*(2), 919–926. https://doi.org/10.1002/2016GL071789

Pan, J., Durand, M., Sandells, M., Lemmetyinen, J., Kim, E. J., Pulliainen, J., et al. (2015). Differences between the HUT snow emission model and MEMLS and their effects on brightness temperature simulation. *IEEE Transactions on Geoscience and Remote Sensing*, *54*(4), 2001–2019. https://doi.org/10.1109/TGRS.2015.2493505

Picard, G., Sandells, M., & Löwe, H. (2018). SMRT: An active-passive microwave radiative transfer model for snow with multiple microstructures and scattering formulations (v1.0). *Geoscientific Model Development*, *11*, 2763–2788. https://doi.org/10.5194/gmd-11-2763-2018

Pirinen, P., Simola, H., Aalto, J., Kaukoranta, J.-P., Karlsson, P., & Ruuhela, R. (2012). *Climatological statistics of Finland 1981–2012. (Report No. 2012-1)*. Finnish Meteorological Institute.

Proksch, M., Mätzler, C., Wiesmann, A., Lemmetyinen, J., Schwank, M., Löwe, H., & Schneebeli, M. (2015). MEMLS3&a: Microwave emission model of layered snowpacks adapted to include backscattering. *Geoscientific Model Development*, *8*, 2611–2626. https://doi.org/10.5194/gmd-8-2611-2015

Pulliainen, J., Grandell, J., & Hallikainen, M. T. (1999). HUT snow emission model and its applicability to snow water equivalent retrieval. *IEEE Transactions on Geoscience and Remote Sensing*, *37*, 1378–1390. https://doi.org/10.1109/36.763302

Pulliainen, J., Kärnä, J. P., & Hallikainen, M. (1993). Development of geophysical retrieval algorithms for the MIMR. *IEEE Transactions on Geoscience and Remote Sensing*, *31*(1), 268–277. https://doi.org/10.1109/36.210466

Pulliainen, J., Luojus, K., Derksen, C., Mudryk, L., Lemmetyinen, J., Salminen, M., et al. (2020). Patterns and trends of Northern Hemisphere snow mass from 1980 to 2018. *Nature*, *581*, 294–298. https://doi.org/10.1038/s41586-020-2258-0

Rautiainen, K., Lemmetyinen, J., Schwank, M., Kontu, A., Menard, C. B., Mätzler, C., et al. (2014). Detection of soil freezing from L-band passive microwave observations. *Remote Sensing of Environment*, *147*, 206–218. https://doi.org/10.1016/j.rse.2014.03.007

Rees, A., Lemmetyinen, J., Derksen, C., Pulliainen, J., & English, M. (2010). Observed and modeled effects of ice lens formation on passive microwave brightness temperatures over snow cover tundra. *Remote Sensing of Environment*, *114*, 116–126. https://doi.org/10.1016/j.rse.2009.08.013

Rott, H., Yueh, S. H., Cline, D. W., Duguay, C., Essery, R., Haas, C., et al. (2010). Cold regions hydrology high-resolution observatory for snow and cold land processes. *Proceedings of the IEEE*, *98*, 752–765. https://doi.org/10.1109/jproc.2009.2038947

Sandells, M., Essery, R., Rutter, N., Wake, L., Leppänen, L., & Lemmetyinen, J. (2017). Microstructure representation of snow in coupled snowpack and microwave emission models. *The Cryosphere*, *11*, 229–246. https://doi.org/10.5194/tc-11-229-2017

Shi, Y., Gao, X., Wu, J., & Giorgi, F. (2011). Changes in snow cover over China in the 21st century as simulated by a high-resolution regional climate model. *Environmental Research Letters*, *6*(4), 045401. https://doi.org/10.1088/1748-9326/6/4/045401

Sihvola, A., & Tiuri, M. (1986). Snow fork for field determination of the density and wetness profiles of a snowpack. *IEEE Transactions on Geoscience and Remote Sensing*, *24*, 717–721. https://doi.org/10.1109/tgrs.1986.289619

Sturm, M., Holmgren, J., & Liston, G. E. (1995). A seasonal snow cover classification system for local to global applications. *Journal of Climate*, *8*(5), 1261–1283. https://doi.org/10.1175/1520-0442(1995)008<1261:ASSCCS>2.0.CO;2

Takala, M., Luojus, K., Pulliainen, J., Derksen, C., Lemmetyinen, J., Kärnä, J.-P., et al. (2011). Estimating Northern hemisphere snow water equivalent for climate research through assimilation of space-borne radiometer data and ground-based measurements. *Remote Sensing of Environment*, *115*(12), 3517–3529. https://doi.org/10.1016/j.rse.2011.08.014

Tan, S., Chang, W., Tsang, L., Lemmetyinen, J., & Proksch, M. (2015). Modeling both active and passive microwave remote sensing of snow using dense media radiative transfer (DMRT) Theory with multiple scattering and backscattering enhancement. *IEEE Journal of Selected Topics in Applied Earth Observations and Remote Sensing*, *8*(9), 4418–4430. https://doi.org/10.1109/jstars.2015.2469290

Tedesco, M., & Narvekar, P. S. (2010). Assessment of the NASA AMSR-E SWE product. *IEEE Journal of Selected Topics in Applied Earth Observations and Remote Sensing*, *3*(1), 141–159. https://doi.org/10.1109/JSTARS.2010.2040462

Werner, C., Wiesmann, A., Strozzi, T., Schneebeli, M., & Mätzler, C. (2010). The SnowScat ground-based polarimetric scatterometer: Calibration and initial measurements from Davos Switzerland. In *IEEE International Geoscience and Remote Sensing Symposium (IGARSS), July 25–30, 2010* (pp. 2363–2366). https://doi.org/10.1109/igarss.2010.5649015

Wiesmann, A., Fierz, C., & Mätzler, C. (2000). Simulation of microwave emission from physically modeled snowpacks. *Annals of Glaciology*, *31*, 397–405. https://doi.org/10.3189/172756400781820453

Wiesmann, A., & Mätzler, C. (1999). Microwave emission model of layered snowpacks. *Microwave Emission Model of Layered Snowpacks*, *70*(3), 307–316. https://doi.org/10.1016/S0034-4257(99)00046-2

Wiesmann, A., Mätzler, C., & Weise, T. (1998). Radiometric and structural measurements of snow samples. *Radio Science*, *33*, 273–289. https://doi.org/10.1029/97rs02746

Wrzesien, M. L., Durand, M. T., Pavelsky, T. M., Kapnick, S. B., Zhang, Y., Guo, J., & Shum, C. K. (2018). A new estimate of North American mountain snow accumulation from regional climate model simulations. *Geophysical Research Letters*, *45*(3), 1423–1432. https://doi.org/10.1002/2017GL076664

Zhu, J., Tan, S., King, J., Derksen, C., Lemmetyinen, J., & Tsang, L. (2018). Forward and inverse radar modeling of terrestrial snow using SnowSAR data. *IEEE Transactions on Geoscience and Remote Sensing*, *56*(12), 7122–7132. https://doi.org/10.1109/TGRS.2018.2848642

Zhu, L., Ives, A. R., Zhang, C., Guo, Y., & Radeloff, V. C. (2019). Climate change causes functionally colder winters for snow cover dependent organisms. *Nature Climate Change*, Vol. *9*, 886–893. https://doi.org/10.1038/s41558-019-0588-4